Received: 7 December 2021 | Revised: 2 May 2022 | Accepted: 19 May 2022

DOI: 10.1002/ecm.1548

ARTICLE

ECOLOGICAL MONOGRAPHS
ECOLOGICAL SOCIETY OF AMERICA

Toward a "modern coexistence theory" for the discrete and spatial

Stephen P. Ellner[1] | **Robin E. Snyder**[2] | **Peter B. Adler**[3] | **Giles Hooker**[4,5]

[1]Department of Ecology and Evolutionary Biology, Cornell University, Ithaca, New York, USA

[2]Department of Biology, Case Western Reserve University, Cleveland, Ohio, USA

[3]Department of Wildland Resources and the Ecology Center, Utah State University, Logan, Utah, USA

[4]Department of Statistics and Data Science, Cornell University, Ithaca, New York, USA

[5]Department of Statistics, University of California, Berkeley, California, USA

Correspondence
Stephen P. Ellner
Email: spe2@cornell.edu

Funding information
National Science Foundation, Grant/Award Numbers: DEB-1933497, DEB-1933561, DEB-1933612

Handling Editor: Marissa Leanne Baskett

Abstract

The usual theoretical condition for coexistence is that each species in a community can increase when it is rare (mutual invasibility). Traditional coexistence theory implicitly assumes that the invading species is common enough that we can ignore demographic stochasticity but rare enough that it does not compete with itself, even after it has reached a stationary spatial distribution. However, short-distance dispersal of discrete individuals leads to locally dense population clusters, and existing theory breaks down. We have an intuition that when we account for invader–invader competition, shorter-range dispersal should reduce the invader's ability to escape competition, but exactly how does this translate into lower population growth? And how will invader discreteness affect outcomes? We need a way of partitioning the contributions to coexistence, but current modern coexistence theory (MCT) does not apply under these conditions. Here we present a computationally based partitioning method to quantify the contributions to coexistence from different mechanisms, as in MCT. We also build up an intuition for how invader clumping and discreteness will affect these contributions by analyzing a case study, a lattice-based spatial lottery model. We first consider fluctuation-dependent coexistence, partitioning the contributions of variable environment, variable competition, demographic stochasticity, and their correlations and interactions. Our second example examines fluctuation-independent coexistence maintained by a fecundity–survival trade-off, and partitions the contributions to coexistence from interspecific differences in fecundity, in mortality, and in dispersal. We find that demographic stochasticity harms an invader, but only slightly. Localized invader dispersal, on the other hand, can have a strong effect. When invaders are more clumped, they compete with each other more intensely when rare, so they too become limited by environment-competition covariance. More invader clumping also means that variation in competition changes from helping the invader to harming it. More broadly, invader clumping is likely to weaken any coexistence mechanism that relies on the invader escaping competition from the resident, because invader clumping means that the resident is no longer the only source of competition.

KEYWORDS
coexistence, coexistence mechanisms, lottery model, modern coexistence theory, niche differences, partitioning, storage effect

INTRODUCTION

We already have spatial coexistence theory for communities in temporally or spatiotemporally varying environments (e.g., Benaim & Schreiber, 2019; Chesson, 2000a; Hening et al., 2021; Snyder et al., 2005; Snyder & Chesson, 2003, 2004), so why do we need more?

Modern coexistence theory (MCT) is based on invasion analysis, which asks whether a species will tend to increase in abundance when it is very rare, either a rare new invader or a previously abundant species reduced to low numbers by a string of bad years or bad luck. Unless each species tends to increase again after becoming rare, persistence of the community is at best fragile and temporary. Theory developed over the last four decades (Benaim & Schreiber, 2019; Chesson, 1982; Chesson & Ellner, 1989; Chesson & Warner, 1981; Hening et al., 2021; Hening & Nguyen, 2018, 2020; Roth & Schreiber, 2014; Schreiber et al., 2011) has confirmed that, in a broad class of models, the coexistence of a set of competing species depends on the ability of each species to increase when it is rare and competing with either the full community or various subsets of the community. The mechanisms allowing a set of species to coexist are then identified by asking what processes or mechanisms give each species a positive population growth rate as a rare invader (Chesson, 1994, 2000a)?

Though a good foundation, this body of theory makes implicit assumptions that are difficult to meet when population dynamics depend on the discrete nature of individuals and their spatial distribution. The first assumption is that demographic stochasticity can be ignored. If we include demographic stochasticity, then the ultimate outcome must always be extinction of one species or the other (though the expected time to extinction may be so long as to be ecologically meaningless). Second, in order for invader growth rate to be a single number, rather than a function of the invader's changing population density, "rare" is assumed to mean that the invader is so rare that it does not compete with itself at all. In technical terms, the model is linearized at zero density for the invader, and the linearized dynamics are used to calculate the invasion growth rate, $\mathbb{E}[r] = \mathbb{E}\log(N(t+1)/N(t))$, where $N(t)$ is the total population of the invader at time t. For populations with spatial structure, existing theory assumes that a successful invader is initially so rare that it converges to a stable spatial structure (at which $\mathbb{E}[r]$ is evaluated) while remaining so rare that the model linearized at zero invader density describes its dynamics; conversely, an unsuccessful invader remains present, even though steadily decreasing in abundance, long enough to reach a stable spatial structure (Benaim & Schreiber, 2019; Chesson, 2000a; Hening et al., 2021; Roth & Schreiber, 2014).

When we apply this theory to real communities, we are simultaneously assuming that the invading species is common enough that we can ignore demographic stochasticity but rare enough that it does not compete with itself, even after it has reached a stationary spatial distribution.

These assumptions are especially problematic in spatially structured communities with discrete individuals. Though a rare species can be microscopically rare in models with continuous population density—and therefore still rare when it has converged to the stable spatial distribution of the linearized model—with discrete individuals that is not possible. The stable spatial distribution for a successful invader will have individuals spread across the entire habitat, so the invader is no longer rare: Invasion growth rates could be computed by linearization at zero density only if individuals are so widely spaced at their stationary distribution that they do not compete, which is possible but not safe as a general assumption. Conversely, an unsuccessful rare invader will likely go extinct before reaching a stable spatial distribution.

Moreover, when there is localized dispersal, the resulting clumping of invaders means that an invading species is likely to affect its own dynamics even when it is still very rare (Figure 1a,b). For example, in a model for the spatial spread of an invader with discrete individuals, Lewis (2000) found that the "key feature slowing spread" (p. 449) below what it would be in the absence of competition was the spatial correlation in the location of related individuals. Spatial clustering of close relatives results from limited parent–offspring distances. Even where the average population density is very low, most individuals are close to some other individual, potentially competing with them directly or producing offspring that will compete with other individuals' offspring. As Figure 1c illustrates, the clumping that results from limited offspring dispersal can have very large effects on the low-density growth rate of a rare invader and, therefore, on its persistence in the community.

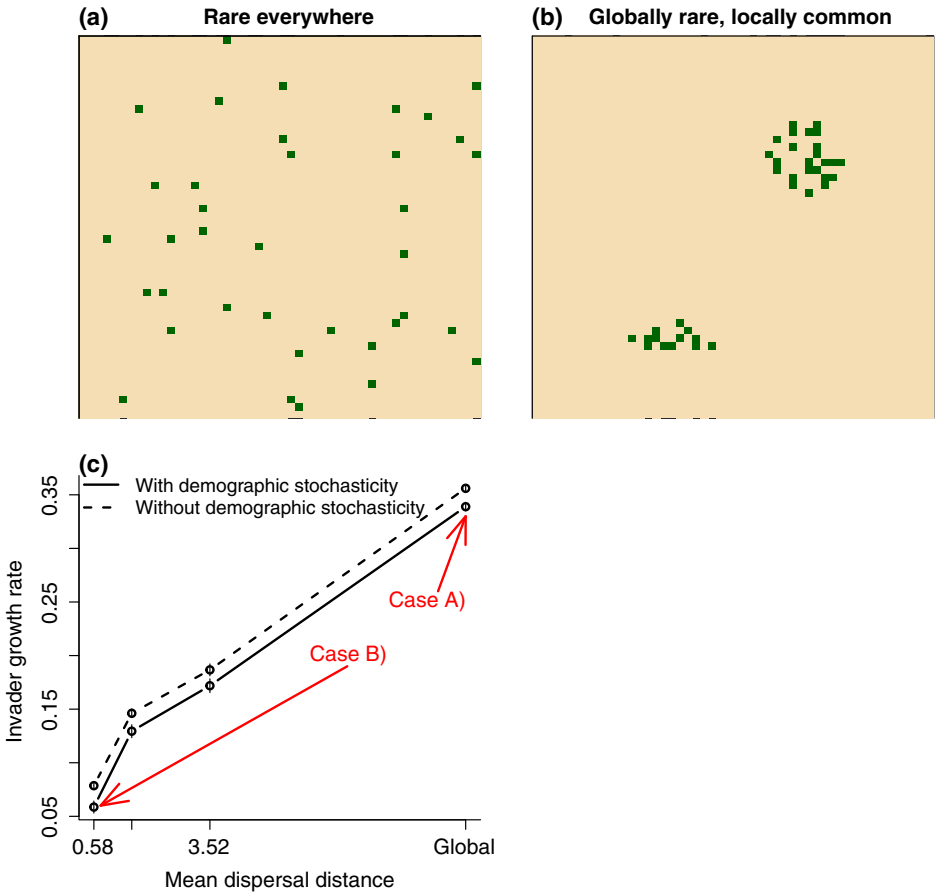

FIGURE 1 Alternative assumptions about the spatial pattern of a rare invader or a species that has become rare due to a string of bad years or bad luck, and their effect on invader growth rate. (a) Existing spatial coexistence theory assumes that a rare species is rare everywhere, spread throughout the habitat so sparsely that it only experiences competition with resident species. (b) In this paper, we consider the case where rare species are modeled as discrete individuals, clumped and locally common enough that a typical individual experiences competitive pressure from nearby conspecifics. (c) Illustration of how clumping (which increases with decreased mean dispersal distance) affects a rare invader's population growth rate, with and without effects of demographic stochasticity, in the lattice lottery model studied in this paper. "Case A" and "Case B" indicate that as mean dispersal distance decreases the population goes from the qualitative scenario illustrated in panel (a) to the scenario in panel (b). Growth rates with demographic stochasticity are from model simulations where adult mortality, and competition among larvae to occupy vacated sites, are stochastic "coin tosses" determining the fate of discrete individuals. Growth rates without demographic stochasticity were calculated from the expected numbers of deaths and sites won. Figure generated by scripts rarity.R and invGrowthVsAlpha.R using R version 4.0.2 or higher.

All populations consist of discrete individuals distributed in space. Nonetheless, we are not arguing that current coexistence theory is universally problematic. If your species of interest is distributed like Figure 1a where and when it is rare, with intraspecific competition weak enough to ignore, then existing theory is valid. However, in many cases, clumping will lead to intraspecific competition even when a species is at the brink of extinction. We need new tools to determine whether such a species is likely to invade and to quantify the mechanisms that influence the invasion's success or failure.

But do we not already have coexistence theory for discrete, spatial models (Durrett, 2002, 2009; Durrett & Levin, 1994)? Yes and no. With rare exceptions (e.g., Chan & Durrett, 2006; Turelli, 1980), in this body of theory demographic stochasticity is the only stochasticity—there is no temporal environmental variability (hence no fluctuation-dependent coexistence mechanisms) and generally no spatial variability. Moreover, nearly all results about coexistence apply only in extremely limited situations: either very long-range interactions between individuals or "rapid stirring," meaning that individuals move randomly on a much faster time scale than births and deaths.

Our eventual goal is a MCT for communities of discrete, locally interacting individuals that addresses all of these limitations. This paper represents a step toward that. Our main topic here is partitioning. We provide methods to quantify the contributions to coexistence from different mechanisms, as in classical MCT, and then

apply those methods to a simple model to start building intuition about how different coexistence mechanisms are affected by invader discreteness and clumping. MCT also addresses the question of what to partition (i.e., whether invader growth rate is a good predictor of coexistence), which we touch on briefly in the *Discussion* section.

To illustrate why partitioning can be informative, consider again Figure 1c. For the model we study here, it shows that shrinking the range of offspring dispersal has a large negative effect on invader growth rate, whereas demographic stochasticity decreases invader growth only slightly (as previously found by Hart et al. [2016]). We have an intuition that because discreteness and clumping result in invader–invader competition even when the invader is globally very rare, shorter-range dispersal should reduce the invader's population growth. But exactly how does that translate into a lower population growth rate? Is it because increased competition reduces the contribution that each coexistence mechanism makes to invader growth rate, or because the invader experiences competition from itself when it is in a good environment, limiting the invader's potential for increase when it is favored over its competitor? Moreover, some coexistence mechanisms do not rely on escaping competition. Relative nonlinearity, for example, asks which species benefits more from (or is less damaged by) the Jensen's inequality effect when competition fluctuates. How much of the decrease (if any) is due to changes in the temporal variance of competition or changes in the degree of nonlinearity in the effect of competition on population growth? Similarly, why does demographic stochasticity have a small effect that is relatively constant as invader clumping varies? Does it have no effect on any coexistence mechanisms, or does it have substantial but opposing effects on different mechanisms? The methods that we develop in this paper make it possible to answer these and similar questions.

The next two sections present background material on the classical lottery model and the functional analysis of variance (fANOVA) approach to partitioning. We then present the discrete, spatial lottery model that we use to demonstrate our methods. The details of our partitioning methods for fluctuation-dependent mechanisms, analogous to Chesson (1994), are presented in the section *Methods: partition based on fluctuation-dependent coexistence mechanisms*. That section begins with a graphical and conceptual overview, allowing readers to skip directly to *Results* and come back for step-by-step instructions if and when they need them. The results for fluctuation-dependent mechanisms are followed by an analysis of coexistence based on life-history differences, for species whose coexistence is not fluctuation-dependent.

BACKGROUND: THE CLASSICAL LOTTERY MODEL AND THE CANONICAL PARTITIONING OF INVASION GROWTH RATE

To explain and demonstrate our approach, we use the simplest model that contains the two key features, discrete individuals and clumping: a spatially explicit version of the lottery model in two-dimensional space. But before we present and study that model, we need to review the classical lottery model and the associated coexistence theory.

The lottery model was originally presented as a model for coral reef fish occupying individual territories (Chesson & Warner, 1981), though it quickly became used for plants and other sessile organisms. We will use the original language, so that new offspring are larvae, but these could just as well be seeds or other propagules. The classical lottery model is based on the following assumptions:

1. The habitat consists of a constant number N of sites, where one adult occupies each site.
2. Each species q adult produces $\beta_q(t)$ larvae in year t, which are dispersed evenly to all sites.
3. Following larval production, some adults die (with mortality rate δ_q). The new occupant at each vacated site is chosen by fair "lottery" among all larvae at the site.

Mathematically, the classical lottery model is a mean field equation for the expected changes in population density given the per-capita fecundities that year. Informally, we think of it as modeling very large populations, with N being a population density (such as sites/km^2). When there are just two species, occupying $N_1(t)$ and $N_2(t)$ sites, respectively, we have $N_1(t) + N_2(t) \equiv N$ and can write the model in terms of $N_1(t)$ as follows:

$$\begin{aligned} N_1(t+1) &= N_1(t)(1-\delta_1) + [\delta_1 N_1(t) + \delta_2(N - N_1(t))] \\ &\quad \times \frac{\beta_1(t) N_1(t)}{\beta_1(t) N_1(t) + \beta_2(t)(N - N_1(t))} \\ &= \text{Survivors} + \text{Number of open sites} \\ &\quad \times \text{Chance to win a site.} \end{aligned} \tag{1}$$

This model does not track discrete individuals, and therefore $N_1(t)$ can have any nonnegative real value.

Coexistence theory for the model involves two steps, invasion analysis and partitioning of invader growth rate.

Invasion analysis

To see if Species 1 persists, we linearize its dynamics at $N_1 = 0$:

$$N_1(t+1) = N_1(t)\left(1-\delta_1+\delta_2\frac{\beta_1(t)}{\beta_2(t)}\right),$$
$$\mathbb{E}[r_1] = \mathbb{E}\log\left(\frac{N_1(t+1)}{N_1(t)}\right) = \mathbb{E}\log\left(1-\delta_1+\delta_2\frac{\beta_1(t)}{\beta_2(t)}\right). \quad (2)$$

Species 1 persists when $\mathbb{E}[r_1] > 0$. (Recall, there is no demographic stochasticity in this model.)

Partitioning

This means that $\mathbb{E}[r_1]$ is expressed as the sum of contributions from different coexistence mechanisms. This can be done in many different ways (Ellner et al., 2019). The canonical decomposition (Chesson, 1994) partitions $\mathbb{E}[r_1]$ into contributions from (i) fluctuation-independent mechanisms, (ii) storage effect, and (iii) relative nonlinearity of competition.

The storage effect consists of contributions to coexistence resulting from density-dependent covariance between environment and competition. Environment E is a measure of the potential for population increase under current conditions, absent competitors. Competition C is a measure of how much worse things really are because competitors are present. For example, the lottery model, Equation (1), can be rearranged into the following form:

$$N_q(t+1) = N_q(t)\left[1-\delta_q+\frac{E_q(t)}{C_q(t)}\right], \quad (3)$$

where

$E_q(t) = \beta_q(t)$, per-capita larval production, and
$1/C_q(t) =$ chance that any one larva becomes an adult, so

$$C_q(t) = \frac{\text{Total no. larvae}}{\text{Total no. open sites}} = \frac{\beta_1(t)N_1(t)+\beta_2(t)(N-N_1(t))}{\delta_1 N_1(t)+\delta_2(N-N_1(t))}. \quad (4)$$

When Species 1 is invading, letting $N_1(t) \to 0$ we get $C_q(t) = \beta_2(t)/\delta_2$ for both species.

To compute the storage effect and other components of invader growth rate, classical MCT uses small-variance quadratic approximations, which require extensive, detailed calculations. We use numerical simulations and fANOVA (Ellner et al., 2019; Hooker, 2007). We start with a simulation of invader population growth with all model parameters set to their observed (fitted) values. We then alter the simulated output to determine how the invader and resident growth rates would change if the world were different. Would the invader's growth rate increase or decrease if the environment were constant instead of variable? What about the resident's growth rate? What if we hold competition constant? What if both environment and competition are constant? What if we break the correlation between environment and competition so they vary independently? We call these scenarios counterfactuals. The right collection of counterfactuals allows us to determine how different features of the model, such as environmental variation, contribute to the invader's growth rate.

Restating this approach in mathematical terms, any multivariate response $\chi(\vec{w})$ can be partitioned exactly as (e.g., Hooker, 2007)

$$\chi(\vec{w}) = \varepsilon_0 + \sum_i \varepsilon_i(w_i) + \sum_{i\neq j}\varepsilon_{i,j}(w_i,w_j) + \cdots + \varepsilon_{1,2,\cdots,d}(\vec{w}). \quad (5)$$

That is,

$$\begin{aligned}\text{Response} = &(\text{Baseline value}) + \Sigma(\text{Main effects})\\ &+\Sigma(\text{2-way interactions})\\ &+\cdots+(d\text{-way interaction}).\end{aligned}$$

We partition invader growth rates based on presence versus absence of particular mechanisms or processes, that is, each w_i in Equation (5) has possible values 1 and 0, indicating presence or absence. Our fANOVA partition of invasion growth rate $\chi = \mathbb{E}[r_i]$ is derived from a set of counterfactual scenarios in which variation or covariation in E or C is absent. Given $r = \log(1-\delta+E(t)/C(t))$, and dropping the species subscript for the moment, we obtain the following:

1. The no-variance baseline is $\varepsilon_0 = r(\overline{E},\overline{C})$.
2. The main effect of variation in E is $\varepsilon_E = \mathbb{E}[r(E,\overline{C})] - \varepsilon_0$.
3. The main effect of variation in C is $\varepsilon_C = \mathbb{E}[r(\overline{E},C)] - \varepsilon_0$.
4. The interaction of variation in E and C is $\varepsilon_{EC} = \mathbb{E}[r(E,C)] - (\varepsilon_0+\varepsilon_E+\varepsilon_C)$.
5. The effect of covariance between E and C is $\varepsilon_\rho = \mathbb{E}[r(E,C)] - \mathbb{E}[r(E^{\#},C)]$; here $E^{\#}$ means that $\mathbb{E}[r]$ is calculated from temporally shuffled $E(t)$ values, so that the marginal distribution of E is the same, but covariation with C is eliminated.

This math is saying that if we measure the invasion growth rate with and without varying E, with C held constant in each, then their difference, ε_E, is the main effect

of letting E vary. Similarly, if we let both E and C vary and measure the invasion growth rate, then if we subtract off the main effects of a variable E, a variable C, and the baseline growth rate in which neither varies, then what is left, ε_{EC}, must be the interaction between a variable E and C. This interaction can be further partitioned by letting E and C vary with their natural correlation, and by breaking that correlation by shuffling the E values, so that the change in invasion growth rate measures the effect of E, C covariance. In Ellner et al. (2019), this idea is explained in more detail and applied to nonspatial models.

E, C covariance benefits a rare species indirectly, by limiting how much a common species can increase in a good year (the enemy of your enemy is your friend!). But to see a "hit" to a resident as a "plus" for the invader, we need to do a term-by-term comparison of growth rate partitions for the invader and for the resident species, as follows:

$$\begin{aligned}\mathbb{E}[r_i] &= \varepsilon_{i,0}+\varepsilon_{i,E}+\varepsilon_{i,C}+\varepsilon_{i,EC}+\varepsilon_{i,\rho}\\ \mathbb{E}[r_r] &= \varepsilon_{r,0}+\varepsilon_{r,E}+\varepsilon_{r,C}+\varepsilon_{r,EC}+\varepsilon_{r,\rho}=0,\end{aligned} \tag{6}$$

where the expected resident growth rate is zero because the resident is at equilibrium. Term-by-term differences (starting with $\varepsilon_{i,0}-\varepsilon_{r,0}=\Delta_{i,0}$) then partition $\mathbb{E}[r_i]-\mathbb{E}[r_r]=\mathbb{E}[r_i]$:

$$\mathbb{E}[r_i]=\Delta_{i,0}+\Delta_{i,E}+\Delta_{i,C}+\Delta_{i,EC}+\Delta_{i,\rho}. \tag{7}$$

Our Δs correspond approximately to Chesson's (1994) coexistence mechanisms, with some caveats discussed in what follows in defining E, C, and demographic stochasticity η, so the classical Chesson (1994) partition is approximately

$$\mathbb{E}[r_i]\approx(\Delta_{i,0}+\Delta_{i,E})+\Delta_{i,C}+\Delta_{i,\rho}. \tag{8}$$

Ellner et al. (2019) found that in models parameterized from experiments, terms omitted from the classical partition can actually be some of the largest. Also, $\Delta_{i,E}$ is a biologically meaningful component of population growth rate (relative nonlinearity in the environment), so we find it informative to keep it separate instead of combining it with $\Delta_{i,0}$.

BACKGROUND: A LATTICE LOTTERY MODEL

We now introduce our focal model, a lottery model with discrete individuals and local offspring dispersal. The environment (maximum per-capita fecundity β_q) varies in time but not in space.

The model's spatial domain is a finite two-dimensional integer lattice consisting of sites $x=(x_1, x_2)$ with $1\le x_1, x_2\le M$, and dynamics occur in discrete time. At times $t=0, 1, 2, \ldots$ each site is either occupied by Species 1 or occupied by Species 2. We let $n_{q,x}(t)$ be the number of species q individuals in site x at time t; possible values are 0 or 1. We assume that all sites vacated by adult mortality are immediately reoccupied.

We assume that competition between adults occurs within a local neighborhood. (Our model is better suited to plants, not fish, but we will continue to use the language of Chesson & Warner [1981] and refer to offspring as larvae.) Specifically, we assume a "top hat" competition kernel, constant within some neighborhood around the focal site and zero outside the neighborhood. The smallest neighborhood we consider is the Moore neighborhood, in which a site's neighbors are the other sites in the 3×3 square centered at the focal site. To explore the effects of longer-range competitive interactions, we consider neighborhoods consisting of the squares of sides 5, 7, and so forth centered on the individual. We refer to the squares of sides 3, 5, 7, and so forth as having competition radius $\rho=1, 2, 3$, and so forth and call them the Moore, Moore2, Moore3, and other neighborhoods. We let $\mathcal{N}_x$ denote the set of sites that are neighbors of x.

Larval dispersal is described by a dispersal matrix $D_{x'|x}$ giving the fraction of larvae produced at site x that land at site x'. We define D through an exponential kernel with a finite-range cutoff. For convenience, following Usinowicz (2015), we let larval dispersal from site x to site x' depend on the sup-norm distance between the sites

$$d(x'|x)=\mathbf{max}\left(|x'_1-x_1|,\ |x'_2-x_2|\right). \tag{9}$$

The Moore neighborhood of a site then consists of all sites at distance $d=1$ from the focal site, the Moore2 neighborhood consists of all sites at distance $0<d\le 2$ from the focal site, and so on. We construct the dispersal matrix so that (ignoring edge effects) the total number of larvae landing at all sites at distance d from the parent is proportional to $e^{-\alpha d}$. The total number of sites at distance d from a focal site far from the lattice margin is $(2d+1)^2-(2d-1)^2=8d$. Thus, with the definition $h(d)=e^{-\alpha d}/(8d)$ the dispersal matrix is

$$D_{x'|x}=\begin{cases}\dfrac{1}{Z_x}h(d(x'|x)) & \text{if } d(x'|x)\le 4,\\ 0 & \text{if } d(x'|x)>4,\end{cases} \tag{10}$$

where Z_x is a constant such that $\sum_{x'}D_{x'|x}=1$. This says in particular that parents near the margins of the habitat

patch do not disperse larvae outside the patch. The cutoff at $d = 4$ is to eliminate any possible artifacts from the long leptokurtic tail of an exponential distribution. Global dispersal is represented by a dispersal matrix in which each parent's larvae are distributed evenly across all lattice sites. The largest possible mean distance for nonglobal dispersal is 2 (resulting from $\alpha = 0$), with larvae dispersed across the 9×9 block centered on the parent such that dispersal distances 0, 1, 2, 3, and 4 are equally likely.

The sequence of events in each time step is as follows:

1. A species q adult in site x—if there is one—produces $F_{q,x}$ larvae. The value of $F_{q,x}(t)$ results from temporally fluctuating maximum per-capita fecundity $\beta_q(t)$ (note that this is spatially constant) possibly modified by local adult competition:

$$F_{q,x}(t) = \frac{\beta_q(t)}{1 + \sum_{s=1}^{2} a_{q,s}\left[z^{-1}\sum_{x' \in \mathcal{N}_x} n_{s,x'}(t)\right]} \tag{11}$$

The quantity in square brackets in the denominator is the fraction of neighbors that are species s, with z the number of neighboring sites ($z = (2\rho + 1)^2 - 1$ for competition radius ρ, for example, $z = 8$ for the Moore neighborhood; recall that a site is not a neighbor of itself). We express competition in terms of the fraction of neighbors, rather than the number of neighbors of each species, so that changing the neighborhood size changes the scale of competition but not the intensity. The coefficients $a_{q,s}$ characterize the strengths of intra- and interspecific competition. In the classical lottery model, $a_{q,s} = 0$ for all q and s. We consider both zero and nonzero competition coefficients to isolate the effects of adult–adult competition and larval competition.

2. The number of species q larvae that land in site x' is then

$$y_{q,x'}(t) = \sum_{x} D_{x'|x} F_{q,x}(t) n_{q,x}(t). \tag{12}$$

Note that the model is deterministic at this step, assuming that the number of larvae is so large that demographic stochasticity in larval dispersal can be ignored.

3. Each species q adult dies with probability $0 < \delta_q < 1$, creating an empty site.
4. If site x' becomes empty, it is occupied by species q with probability

$$\frac{y_{q,x'}(t)}{y_{1,x'}(t) + y_{2,x'}(t)}. \tag{13}$$

As noted earlier, we start simulations with all sites occupied, so $y_{1,x'}(t) + y_{2,x'}(t)$ is always positive.

METHODS: PARTITION BASED ON FLUCTUATION-DEPENDENT COEXISTENCE MECHANISMS

Our goal in this section is to develop a partition of invader growth rate for discrete, spatial models that is as closely analogous as possible to the canonical partitioning for the nonspatial model (Chesson, 1994, 2000b) and in addition takes into account the effect of demographic stochasticity.

To accomplish that, we had to address a series of questions:

1. How should we define the environment measure E, competition C, and demographic stochasticity η for the lattice lottery model?
2. How should we define the invasion growth rate $\mathbb{E}[r]$?
3. We concluded that the right measure of $\mathbb{E}[r]$ is the average per-capita invader growth rate when the invader is distributed in small clusters. How can we generate a sample of lattice configurations with small invader clusters?
4. How do we evaluate the invasion growth rate $\mathbb{E}[r]$ for that sample?
5. How do we partition $\mathbb{E}[r]$ into contributions from difference coexistence mechanisms?

Our approach is summarized in Figure 2 and Box 1. Please look first at Figure 2, which summarizes the simulations that are used to estimate and partition invader growth rate. Invader growth rate is quantified as the average change in the log of total invader population over one time step when the invader is distributed in isolated small clusters.

We simulate the model up to some large time T, resetting the lattice as necessary to maintain small invader clusters (we explain below how this was done). For each lattice configuration at time T, we do replicate simulations of the populations at time $T + 1$, recording E, C, and η for each simulation. We then use these recorded values to calculate the counterfactual invader and resident growth rates that would have occurred if one or more of E, C, and η were set to their time-averaged values (see Figure 3 for some examples). Equation (27) details

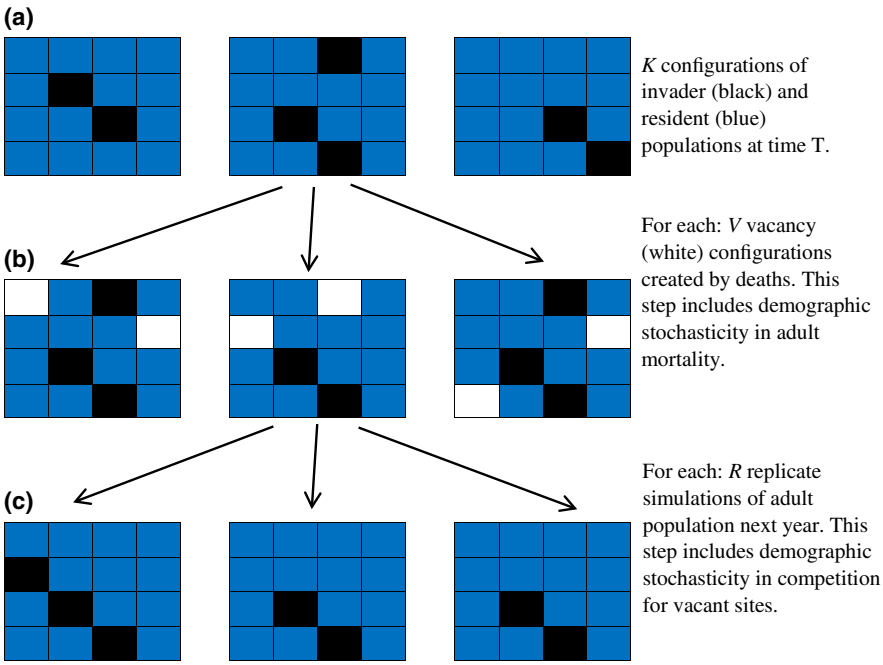

FIGURE 2 Schematic summary of one-step-ahead simulations that provide the information needed for the partition. Black indicates a site occupied by an adult of the invading species; blue, a site occupied by a resident species adult; and white, a vacant site. Separating one time step into the two stages depicted above is only required for considering separately the effects of demographic stochasticity in adult mortality and in the lottery for vacated sites. (a) Do replicate simulations up to time $T \gg 1$ to generate K configurations of resident and invader adults in the lattice. For each record $\overline{S}_q$, the expected number of adults in each species that will survive to the next year. (b) For each configuration do V replicate coin-tossing simulations of adult mortality creating vacant sites. For each record S_q, the actual number of adults that survived in each species. (c) For each of the KV adult/vacancy configurations, do R replicate simulations of larval competition for vacant sites: Choose environments E_q, disperse larvae, and choose the winner at each vacant site. These outcomes are used to compute measures of competition C_q and demographic stochasticity η_q, as explained in the main text. Because demographic stochasticity has very small effects in our model, we do not distinguish between the two kinds of demographic stochasticity. For that case, it is simplest to take $R = 1$ and do V complete one-step-ahead simulations from each adult configuration at time T.

how these counterfactual growth rates are used to partition both the invader and resident growth rates. Finally, Equation (28) shows the term-by-term comparison of invader and resident partitions that creates the fANOVA partitioning of invader growth rate.

Like all MCT partitions of contributions from different coexistence mechanisms, this is a retrospective analysis: For an observed instance of coexistence, it identifies the contributing mechanisms and how much each contributes. A prospective analysis, in contrast, would predict whether or not a set of species will coexist based on intrinsic properties of each species (e.g., thermal tolerances) that could be quantified outside the context of a community where all coexist.

The rest of this section gives the details of these procedures and provides explicit formulas for all of the calculations. If and when you want to do this yourself, or you really want to know the details, you need to read the rest of this section. Readers more interested in the general approach and the results can focus on Box 1 and Figure 2 and then skip to the section *Results: partition based on fluctuation-dependent coexistence mechanisms* to see the payoffs.

Defining E, C, and demographic stochasticity η

Our definitions of E, C and η are based on the following principles:

1. E and C determine the expected population change given the state of the lattice. The effects of demographic stochasticity are defined in terms of deviations from this expected value.
2. We define E and C as biologically interpretable aspects of the model rather than using the "standard parameters" $\mathcal{E}, \mathcal{C}$ that analytic MCT introduces to simplify quadratic approximations.
3. We also do not use the comparison coefficients q_{ir} from analytic MCT, which are chosen to zero out a term in the quadratic approximation. Instead, we develop

BOX 1 Conceptual recipe for an invasion growth rate partition based on fluctuation-dependent mechanisms, analogous to the classical analysis of the nonspatial lottery model.

1. Define environment E (per-capita fecundity in absence of competition), competition C limiting actual recruitment, and demographic stochasticity η, so that the dynamics of the total invader population N can be written

$$N(t+1) = [(1-\delta)N(t) + N(t)E(t)/C(t)]\eta(t). \quad (29)$$

   Although nothing in Equation (29) is explicitly spatially dependent, the values of E, C, and η reflect how the spatial distribution of each species influences fecundity, competition, and demographic stochasticity.
2. Through simulations (Figure 2) evaluate E, C, and η for all $K \times V \times R \gg 1$ one-step-ahead model simulations.
3. For each simulation there is a true value of a population growth measure χ such as $r = \log(N(t+1)/N(t))$.
4. Partition $\overline{\chi}$, the average of χ across all simulations, into contributions from different mechanisms. We do that by evaluating the effects of Var (C), Var (E), Cov (E, C), Var (η), and their interactions on the invader and resident population growth rates through a series of counterfactuals in which some aspects of the real invasion dynamics are present while others have been removed—see Figure 3 for some examples. The resulting partition is given by Equation (27).
5. Use the simulation results (Step 2) to evaluate the necessary counterfactuals. For example, for the counterfactual situation in Figure 3C where there is only variation in E, we set all $C(t)$ values to $\overline{C}$ (the average C value across all one-step-ahead simulations), set all $\eta(t)$ values to $\overline{\eta}$, use those to recompute $N(t+1)$ values for each one-step-ahead simulation using Equation (29), and use the new $N(t+1)$ values to recompute $\overline{\chi}$. This tells us what $\overline{\chi}$ would have been had only E been varying while C remained constant at its observed mean.
6. As in the nonspatial model, coexistence mechanisms are calculated as term-by-term differences between the partitions of invader and resident growth rates, Equation (28).

methods for pairwise comparisons between an invader and each resident species as in Ellner et al. (2019), because this provides more information than the classical approach of comparing the invader's growth rate to a weighted average of resident growth rates.

Defining E_q

As in the standard lottery model, we define $E_q = \beta_q$.

Defining C_q

For the standard lottery model C_q is the ratio by which the total number of new larvae $N_q E_q$ is reduced by competition, to give the number of new recruits. We want $C_q(t)$ to have the same meaning in our lattice model. Based on the foregoing Principle 1, we define $C_q(t)$ to be the ratio between the number of new larvae $N_q(t)E_q(t)$ and the expected number of species q new recruits at time $t+1$, $\overline{R}_q(t+1)$, conditional on the lattice state and the environments $E_q(t)$

$$C_q(t) = \frac{\beta_q(t)N_q(t)}{\overline{R}_q(t+1)}. \quad (14)$$

When $\beta_q(t) = 0$, also $\overline{R}_q(t+1) = 0$, and so $C_q(t)$ is defined to be the limit of Equation (14) as $\beta_q(t) \to 0$. The somewhat complicated formulas for calculating $\overline{R}_q$ and C_q are derived in Appendix S1: Section S1.

These are not the only possible choices for E and C; for example, the logs of our E and C could be used instead, or any other monotonic transformation preserving the property that large E is good for population growth, and large C is bad. Different choices will affect the baseline (no fluctuations) growth rate (because the mean of $\log(E)$ is not the log of mean E), and therefore the main effects of variance in E and C. We do not argue that any one choice is "best." All such choices give valid partitions, and it may be informative to do several different partitions.

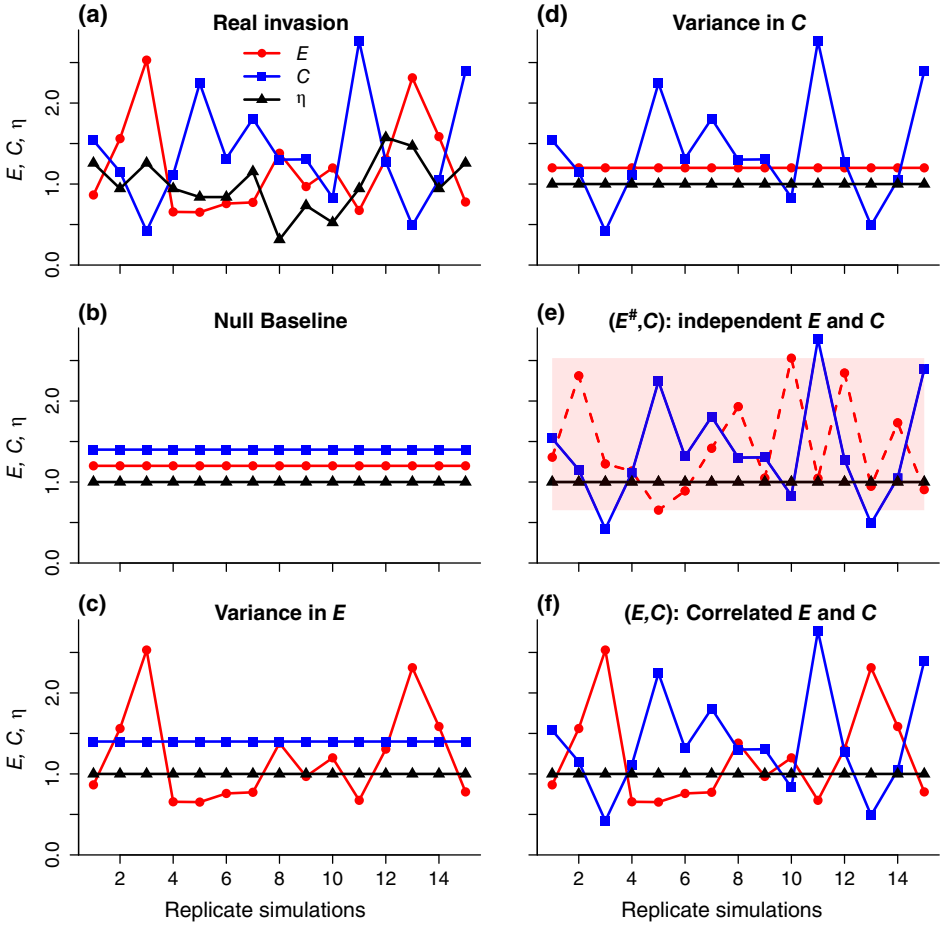

FIGURE 3 Conceptual illustration of some counterfactuals used to evaluate different fluctuation-dependent mechanisms. (a) Simulations with all mechanisms present. (b) Baseline "null" where E, C, and η are set to their means across simulations. (c) Variance in E only—this lets us evaluate the main effect of Var(E). (d) Variance in C alone—this lets us evaluate the main effect of Var(C). (e) Uncorrelated variance in both E and C generated by drawing a new realization of $E(t)$ values from the assumed distribution (indicated by shading)—this lets us evaluate the interaction between variance in E and variance in C. (f) Correlated variance in both E and C—the difference between this case and e) lets us evaluate the effect of E, C covariance. Figure made by script PartitionSchematicFigure.R using R version 4.1.1.

Separating the effects of demographic stochasticity

To do this, we write $N_q(t+1)$ as the product of its expected value—given the lattice configuration at time t and the environments $E_q(t)$—with a deviation $\eta_q(t)$ resulting from demographic stochasticity in adult mortality and the lottery at vacated sites. The expected number of current adults in species q that are still alive at time $t+1$ is

$$\overline{S}_q(t+1) = \mathbb{E}\sum_x (1 - V_x(t)) = (1-\delta_q)N_q(t). \quad (15)$$

The conditional expected population at $t+1$ is $\overline{S} + \overline{R} = \overline{S} + NE/C$, so we set

$$N_q(t+1) = \left[\overline{S}_q(t+1) + N_q(t)E_q(t)/C_q(t)\right]\eta_q(t). \quad (16)$$

Note that Equation (16) is the definition of $\eta_q(t)$ and the formula for computing it. Given the lattice state and environments at time t, the expression in square brackets, which is the conditional expectation of $N_q(t+1)$, is known. $N_q(t+1)$ is a simulation output resulting from coin tossing at each site to see if the adult dies and coin tossing at each vacated site to determine the lottery winner. The ratio between the conditional expectation and the simulated outcome is the demographic stochasticity effect $\eta_q(t)$.

Having defined the terms so that the population dynamics can be written in the form of Equation (16), in principle we can again carry out the partitioning given by

Equation (7), with an additional main effect for demographic stochasticity η and the resulting additional interaction terms. A crucial difference, however, is that for the spatial model we cannot sample C_q and η_q from known distributions—we have to use simulations to generate samples from their distributions and average across those samples to estimate the terms in Equation (7). The following sections explain how those are accomplished.

Defining the invasion growth rate $\mathbb{E}[r]$

There is considerable mathematical theory on long-term population expansion patterns in spatial models with continuous population density (reviewed by Kot [2003] and Lutscher [2019]) or with discrete individuals (e.g., Allstadt et al., 2007; Bessonov & Durrett, 2017; Cox & Durrett, 1988; Durrett, 1988; Gandhi et al., 1999; Korniss & Caraco, 2005; Kot et al., 2006; Lewis, 2000; O'Malley et al., 2006, 2009; Reluga, 2016; Snyder, 2003)—often the long-term behavior is a traveling wave with asymptotically constant velocity in one dimension and in two dimensions an expanding disc with asymptotically constant radial rate of increase. Based on existing theory, we initially thought that the initial invader population growth rate in our model would reflect the expansion of small clusters with a constant rate of radial growth. In that case, the square root of invader population, which is proportional to cluster radius, would show a constant rate of increase over time. But this turned out to be wrong—possibly because previous theory with discrete individuals typically assumed that offspring only dispersed to nearest-neighbor sites. For the model we consider here, our simulation experiments suggest that the best measure of initial spread is, somewhat surprisingly, still $\mathbb{E}[r]$, the expected change in log total population over one time step, for lattice states where the invader's abundance is in a range where $\mathbb{E}[r]$ is approximately constant as a function of invader abundance.

As we discuss in Appendix S1: Section S2, the last statement is specific to our particular model, not about spatial models in general, and it is a statement qualified by the fact that the supporting evidence comes entirely from simulations. The standard lottery model uses the same invasion growth rate measure, with one difference. For the standard lottery model it is computed for an infinitesimally rare invader by linearizing the model around zero invader abundance. Here we consider $\mathbb{E}[r]$ when the invader total abundance is in some range $[G_{\min}, G_{\max}]$, where $G_{\min}$ is large enough that extinction in one time step is so unlikely that it never actually occurs in simulations, and $G_{\max}$ is small enough that population growth is not appreciably reduced by the slightly greater intraspecific competition that is observed to occur in larger clusters. In practice we used $G_{\min} = 10$, $G_{\max} = 40$. Simulation results (Appendix S1: Figure S3) show that over that range, the slope of $\mathbb{E}[r]$ with respect to invader abundance N is ≈ 0.01 of the mean value of $\mathbb{E}[r]$. As we have emphasized, the combination of discrete individuals and clumping means that even in small clusters, invaders experience intraspecific competition. An ideal measure of invader population growth would become completely independent of invader population as the invader becomes increasingly rare. That ideal appears not to exist for our model—the limit of rarity is a single invader experiencing no intraspecific competition, which is not typical of small invader clusters—but average $\mathbb{E}[r]$ for N in $[G_{\min}, G_{\max}]$ comes very close to the ideal.

Generating a sample of lattice configurations with small invader clusters

We thus need a sample of lattice configurations with invader total abundance in the target range $[G_{\min}, G_{\max}]$. We cannot just let the residents come to a stationary distribution and sprinkle in a few invaders: The whole purpose of this paper is to address situations where invader aggregation matters, so we need a realistic invader cluster structure. The ideal method would be to simulate the model long enough to wipe out the effects of the initial population state, simulate further until the invader enters and then leaves the target range, and randomly choose one of the lattice states in the target range—repeat K times. However, that approach is computationally infeasible because a species that coexists in a community will rarely enter the target range, where its abundance will be far below average.

We therefore used the following shortcut. Whenever the invader population went extinct or exceeded a threshold $N_{\max} > G_{\max}$, we restarted the simulation from the original initial conditions, which had $N_{\min} < G_{\min}$. In all our simulations, $N_{\max}$ was at least $2G_{\max}$, and $N_{\min} = 4$ (one 2×2 cluster). The rationale for this shortcut is that by the time a simulation gets to the target range $[G_{\min}, G_{\max}]$, it will have "forgotten" how it was restarted, so invader population states in the target range will be equivalent to those arising in a very long simulation without restarts.

Because this repeated-invasions approach is a shortcut, we compared the lattice configurations that it generated with those generated in a different way, using a version of the Fleming–Viot algorithm for sampling from quasi-stationary distributions (e.g., Asselah et al., 2011; Groisman & Jonckheere, 2013). This method, and the evidence that it gives samples equivalent to those from our repeated invasions shortcut, is presented in Appendix S1: Section S3.

Replicate simulations were initialized with a single 2×2 cluster of invaders and were run in parallel for long enough that replicates were uncorrelated because each

had been reinitialized many times ($T = 500$ or more). Sufficient replicates were run (generally 250 or more) so that at least 50 ended with the invader population in the target range for all parameter values considered.

Evaluating $\mathbb{E}[r]$ for a given lattice configuration

For each of the K replicate lattice configurations at time T (indexed by k for "konfiguration"), we compute the vacancy probability $V_x^{(k)}(T)$ for each lattice site, as defined earlier, and the expected number of surviving adults $\overline{S}_q^{(k)}(T+1)$ for each species.

For each configuration k, V different configurations of site vacancies (indexed by v) are randomly generated according to the species-specific mortality rates. For each k, v pair we record $S_q^{(v|k)}(T+1)$, the actual number of adults in each species surviving to time $T+1$. We will use this to calculate the new resident and invader populations in the next step.

For each (k, v) combination, we do R one-step-ahead simulations (indexed by r) to compute population sizes at time $T+1$ starting from the resident-invader configuration k and vacancy configuration v. Each such simulation starts by drawing a new set of random values of the environment variables for each species, $\beta_q^{(r|v,k)(T)}$; we add the r, v, and k superscripts to $\beta_q(T)$ to indicate that there is an independent environment value for each replicate. Using those, we compute larval production by each adult, compute the larvae landing at each site $y_{q,x}^{(r|v,k)}(t)$, draw a winner at each vacant site, and record the resulting total population of each species $N_q^{(r|v,k)}(T+1)$. Note that the new population $N_q^{(r|v,k)}(T+1)$ depends on the actual number of survivors $S_q^{(v|k)}(T+1)$ recorded for each vacancy configuration. Because larval production occurs before adult mortality in our model, larval production actually depends on k and r but not v, but we include the v index in our general procedure to allow for models where nearby adults might affect larval dispersal or survival.

For each (k, v, r) combination we use Appendix S1: Equation S2 to compute $\overline{R}_q^{(r|v,k)}(T+1)$, and then

$$C_q^{(r|v,k)}(T) = \frac{\beta_q^{(r|v,k)}(t) N_q^{(k)}(T)}{\overline{R}_q^{(r|v,k)}(T+1)},$$
$$\eta_q^{(r|v,k)}(T) = \frac{N_q^{(r|v,k)}(T+1)}{\left[\overline{R}_q^{(r|v,k)}(T+1) + \overline{S}_q^{(k)}(T+1)\right]}. \quad (17)$$

For each of the KVR one-step-ahead simulations we store the values of $E_q^{(r|v,k)}(T)$, $C_q^{(r|v,k)}(T)$, $\overline{R}_q^{(r|v,k)}(T+1)$, $\eta_q^{(r|v,k)}(T)$, the initial and final population sizes, and the measure of the population growth between T and $T+1$, which we denote $\chi_q^{(r|v,k)}$. In this paper, χ is always the change in the log of total population, but for generality we present the formulas in terms of a general growth measure χ. We also need to compute and store for each configuration k any measures of spatial structure that we might want to use as covariates in a regression analysis of how spatial structure affects the magnitude of different "mechanisms." However, it is not necessary to save the complete lattice state, which would be memory-intensive, because the calculations needed for the fANOVA decomposition can all be done using the stored η, E, C, χ, and N values and spatial summary statistics.

The overall estimate of the population growth measure χ_q is

$$\overline{\chi}_q(E, C, \eta) = \frac{1}{KVR} \sum_{k=1}^{K} \sum_{v=1}^{V} \sum_{r=1}^{R} \chi_q^{(r|v,k)}(E, C, \eta) \quad (18)$$

where the (E, C, η) notation means that the value of χ_q is computed for the actual stored E, C, and η values for each species.

Partitioning $\mathbb{E}[r]$ into contributions from difference coexistence mechanisms

Exactly as for the standard lottery model (Ellner et al., 2019), the partition is based on applying the general fANOVA decomposition given by Equation (5) to invader and resident population growth rates, based on counterfactual population growth rates when particular processes or mechanisms are removed (Figure 3). These counterfactual growth rates are calculated by altering components of the one-step-ahead population changes expressed in the form

$$N_q^{(r|v,k)}(T+1) = \left[\overline{S}_q^{(k)}(T+1) + N_q^{(k)}(T)\frac{E_q^{(r|v,k)}(T)}{C_q^{(r|v,k)}(T)}\right]\eta_q^{(r|v,k)}(T). \quad (19)$$

The necessary counterfactuals are as follows:

1. To create the $\overline{E}$ counterfactual, for each (r, v, k), compute a pseudo-one-step-ahead population change as

$$N_q^{(r|v,k)}(T+1) = \left[\overline{S}_q^{(k)}(T+1) + N_q^{(k)}(T)\frac{\overline{E}_q}{C_q^{(r|v,k)}(T)}\right]\eta_q^{(r|v,k)}(T), \quad (20)$$

where $\overline{E}_q$ is either the average of all $E_q^{(r|v,k)}(T)$ values or the theoretical mean of the distribution from which E_q is

drawn. For each (r, v, k), use the pseudo-one-step-ahead population value given by Equation (20) to compute a population change measure $\chi_q^{(r|v,k)}(\overline{E}, C, \eta)$, where the $\overline{E}$ indicates that the calculations were done using average E values. The counterfactual population change measure is then

$$\overline{\chi}_q(\overline{E}, C, \eta) = \frac{1}{KVR}\sum_{k=1}^{K}\sum_{v=1}^{V}\sum_{r=1}^{R}\chi_q^{(r|v,k)}(\overline{E}, C, \eta). \quad (21)$$

2. The $E^{\#}$ counterfactual requires breaking (E, C) covariance without changing marginal distributions. To do this, for every (r, v, k) combination, draw a new set of E values for each species, $E_q^{\#(r|v,k)}(T)$. Then compute the pseudo-one-step-ahead population changes as

$$N_q^{(r|v,k)}(T+1) = \left[\overline{S}_q^{(k)}(T+1) + N_q^{(k)}(T)\frac{E_q^{\#(r|v,k)}(T)}{C_q^{(r|v,k)}(T)}\right]\eta_q^{(r|v,k)}(T) \quad (22)$$

and compute the resulting population change measure $\chi_q^{(r|v,k)}(E^{\#}, C, \eta)$. The average of these *RVK* values gives the counterfactual population change measure $\overline{\chi}_q(E^{\#}, C, \eta)$.

3. To compute the $\overline{C}$ counterfactual (completely constant competition), for each species, compute

$$\overline{C}_q(T) = \frac{1}{KVR}\sum_{k=1}^{K}\sum_{v=1}^{V}\sum_{r=1}^{R}C_q^{(r|v,k)}(T). \quad (23)$$

Then for each (r, v, k), compute the pseudo-one-step-ahead population change as

$$N_q^{(r|v,k)}(T+1) = \left[\overline{S}_q^{(k)}(T+1) + N_q^{(k)}(T)\frac{E_q^{(r|v,k)}(T)}{\overline{C}_q(T)}\right]\eta_q^{(r|v,k)}(T) \quad (24)$$

and compute the resulting population change measure $\chi_q^{(r|v,k)}(E, \overline{C}, \eta)$. The average of these *RVK* values gives the counterfactual population change measure $\overline{\chi}_q(E, \overline{C}, \eta)$.

4. To compute the $\overline{\eta}$ counterfactual, for each species, compute

$$\overline{\eta}_q(T) = \frac{1}{KVR}\sum_{k=1}^{K}\sum_{v=1}^{V}\sum_{r=1}^{R}\eta_q^{(r|v,k)}(T), \quad (25)$$

which should be approximately 1. Then, for each (r, v, k), compute the pseudo-one-step-ahead population change as

$$N_q^{(r|v,k)}(T+1) = \left[\overline{S}_q^{(k)}(T+1) + N_q^{(k)}(T)\frac{E_q^{(r|v,k)}(T)}{C_q(T)}\right]\overline{\eta}_q^{(r|v,k)}(T) \quad (26)$$

and compute the resulting population change measure $\chi_q^{(r|v,k)}(E, C, \overline{\eta})$. The average of these *RVK* values gives the counterfactual population change measure $\overline{\chi}_q(E, C, \overline{\eta})$.

We now have all the necessary ingredients to partition $\overline{\chi}_q(E, C)$ using Equation (5):

$$\begin{aligned}
\overline{\varepsilon}_q^{0} &= \overline{\chi}_q(\overline{E}, \overline{C}, \overline{\eta})\\
\overline{\varepsilon}_q^{E} &= \overline{\chi}_q(E, \overline{C}, \overline{\eta}) - \overline{\varepsilon}_q^{0}\\
\overline{\varepsilon}_q^{C} &= \overline{\chi}_q(\overline{E}, C, \overline{\eta}) - \overline{\varepsilon}_q^{0}\\
\overline{\varepsilon}_q^{\eta} &= \overline{\chi}_q(\overline{E}, \overline{C}, \eta) - \overline{\varepsilon}_q^{0}\\
\overline{\varepsilon}_q^{EC} &= \overline{\chi}_q(E, C, \overline{\eta}) - \left(\overline{\varepsilon}_q^{E} + \overline{\varepsilon}_q^{C} + \overline{\varepsilon}_q^{0}\right)\\
\overline{\varepsilon}_q^{E\sharp C} &= \overline{\chi}_q(E^{\#}, C, \overline{\eta}) - \left(\overline{\varepsilon}_q^{E} + \overline{\varepsilon}_q^{C} + \overline{\varepsilon}_q^{0}\right)\\
\overline{\varepsilon}_q^{\mathrm{Cov}(E,C)} &= \overline{\chi}_q(E, C, \overline{\eta}) - \overline{\chi}_q(E^{\#}, C, \overline{\eta})\\
\overline{\varepsilon}_q^{E\eta} &= \overline{\chi}_q(E, \overline{C}, \eta) - \left(\overline{\varepsilon}_q^{E} + \overline{\varepsilon}_q^{\eta} + \overline{\varepsilon}_q^{0}\right)\\
\overline{\varepsilon}_q^{E\sharp\eta} &= \overline{\chi}_q(E^{\#}, \overline{C}, \eta) - \left(\overline{\varepsilon}_q^{E} + \overline{\varepsilon}_q^{\eta} + \overline{\varepsilon}_q^{0}\right)\\
\overline{\varepsilon}_q^{\mathrm{Cov}(E,\eta)} &= \overline{\chi}_q(E, \overline{C}, \eta) - \overline{\chi}_q(E^{\#}, \overline{C}, \eta)\\
\overline{\varepsilon}_q^{C\eta} &= \overline{\chi}_q(\overline{E}, C, \eta) - \left(\overline{\varepsilon}_q^{C} + \overline{\varepsilon}_q^{\eta} + \overline{\varepsilon}_q^{0}\right)\\
\overline{\varepsilon}_q^{EC\eta} &= \overline{\chi}_q(E, C, \eta) - \left(\overline{\varepsilon}_q^{E\eta} + \overline{\varepsilon}_q^{EC} + \overline{\varepsilon}_q^{C\eta} + \overline{\varepsilon}_q^{E} + \overline{\varepsilon}_q^{C} + \overline{\varepsilon}_q^{\eta} + \overline{\varepsilon}_q^{0}\right).
\end{aligned} \quad (27)$$

We could also have decomposed $\overline{\varepsilon}_q^{C\eta}$ into variance and covariance effects, but we chose not to. Note that the effect of covariance between two factors is evaluated by comparison to the counterfactual in which those two factors are independent but retain their marginal distributions, while all other factors are constant. If the marginal distributions are not known, those counterfactuals can be implemented by randomization (Ellner et al., 2016).

Having done the growth rate partition given by Equation (27) for invading species i and resident species s, we define $\Delta_i^{\bullet} = \overline{\varepsilon}_i^{\bullet} - \overline{\varepsilon}_s^{\bullet}$. The fANOVA partition of invader growth rate into coexistence mechanisms is

$$\begin{aligned}
\overline{\chi}_i(E, C) = \Delta_i^{0} + \Delta_i^{E} + \Delta_i^{C} + \Delta_i^{E\sharp C} + \Delta_i^{\mathrm{Cov}(E,C)} + \Delta_i^{E\sharp\eta}\\
+ \Delta_i^{\mathrm{Cov}(E,\eta)} + \Delta_i^{C\eta} + \Delta_i^{EC\eta}.
\end{aligned} \quad (28)$$

Finer partitions are possible. For example, the $\overline{C}$ counterfactual of Equation (23) washes out all information about how spatial structure affects the distribution of C values. To preserve some of that information, we could consider an intermediate counterfactual where each "real" C_q value is replaced by its average for the particular invader–resident configuration—this retains variation in average C between different configurations but removes variance within each configuration. We explain how to do this calculation in Appendix S1: Section S4.

As in Ellner et al. (2019), we consider only the direct effect of fluctuations. Indirect effects can be mediated via changes in the size structure of the population or, here, in changes to the lattice configuration. We originally thought we could include indirect effects by generating new lattice states for each counterfactual, but this is not feasible: What would it mean (for example) to simulate the model to time T with covariance between E and C removed? C is an overall measure of how much competition suppresses population growth. In a nonspatial model with continuous population density, we can remove E, C covariance by drawing a C value at each time step from the marginal distribution of C in the full model (Ellner et al., 2016) and using that C value to compute next year's population. But in our discrete spatial model, doing the same does not give us the spatial configuration of individuals, which is essential information for taking future time steps and generating the necessary lattice states at time T.

RESULTS: PARTITION BASED ON FLUCTUATION-DEPENDENT COEXISTENCE MECHANISMS

We now use our partitioning method to dissect an example of fluctuation-dependent coexistence in the lattice lottery model. The upper panel of Figure 4 shows the $\overline{\varepsilon}$ partitions (Equation 27) for both species. Parameter values (given in the caption) are such that the invader (Species 2) and resident (Species 1) are identical, except that the invader's mean fecundity is slightly lower, so in the absence of fluctuations or intraspecific competition the invader could not persist. These results show that tighter invader clustering (resulting from lower larval dispersal distance) has little effect on the components of resident population growth rate, but for the invader the baseline (no-fluctuations) growth rate is slightly larger, variation in C is less helpful, and Cov(E, C) is more harmful. Demographic stochasticity η has a weak negative effect on the invader that is larger for wider larval dispersal but has no effect on the resident. An equivalent barplot for mortality rate $\delta = 0.1$, showing similar results, can be found in Appendix S1: Section S6.

The lower panel of Figure 4 shows the resulting invasion growth rate partition (Equation 28) for Species 2. With decreasing larval dispersal distance, relative nonlinearity of competition (Var C) hurts the invader more (relative to the resident), the storage effect (Cov[E, C]) helps the invader less, and demographic stochasticity hurts the invader slightly less. We thus find—answering one question we posed in the introduction—that the reduction in invader growth rate with shorter-range larval dispersal results from two factors: decreasing benefit from the storage effect and increasing harm from relative nonlinearity of competition, partially offset by an increase in the baseline no-fluctuations growth rate.

Let us explore these results a little further. Figure 5 shows that the strength of the temporal storage effect is largely determined by the mortality rate δ and by the average larval invader fraction, the average fraction of a randomly chosen invader larva's fellow larvae within its site that are conspecifics. (This is essentially Lloyd's mean crowding index, applied to invader larvae.) Average larval invader fraction is a useful measure of invader clumping and intraspecific competition: If invaders are clumped and dispersal is local, then an invader larva is likely to find itself accompanied by larvae from other nearby invader parents, rather than resident species larvae.

To assess the impact of other model parameters, we therefore ask how they affect average larval invader fraction. By fitting linear models with average larval invader fraction as the response and model parameters as explanatory variables (see script AnovaAnalyses.R), we find that 91% of the variance in average larval invader fraction is explained by the main effects of dispersal parameter α (83% of the total sum of squares) and adult competition a (7%); the interaction between α and a explains an additional <1%. Surprisingly, mortality rate δ had no detectable effect on the average larval invader fraction. Both α and a have positive regression coefficients: Higher values of both increase invader crowding and weaken the storage effect. The effect of α is intuitive: More localized dispersal increases crowding. We might expect higher adult competition a to decrease invader crowding by increasing the spacing between adults, but it actually leads to the opposite. We suspect that this is because the biggest effect of intraspecific competition is to decrease resident average fecundity, thereby decreasing the average number of resident larvae in each site.

ΔC is also strongly affected by the average larval invader fraction (Figure 6), but the relationship is less tight than that for ΔCov(E,C). The average larval invader fraction explains 50% of the total sum of squares, but in addition a explains 21% and δ explains 15% (see script

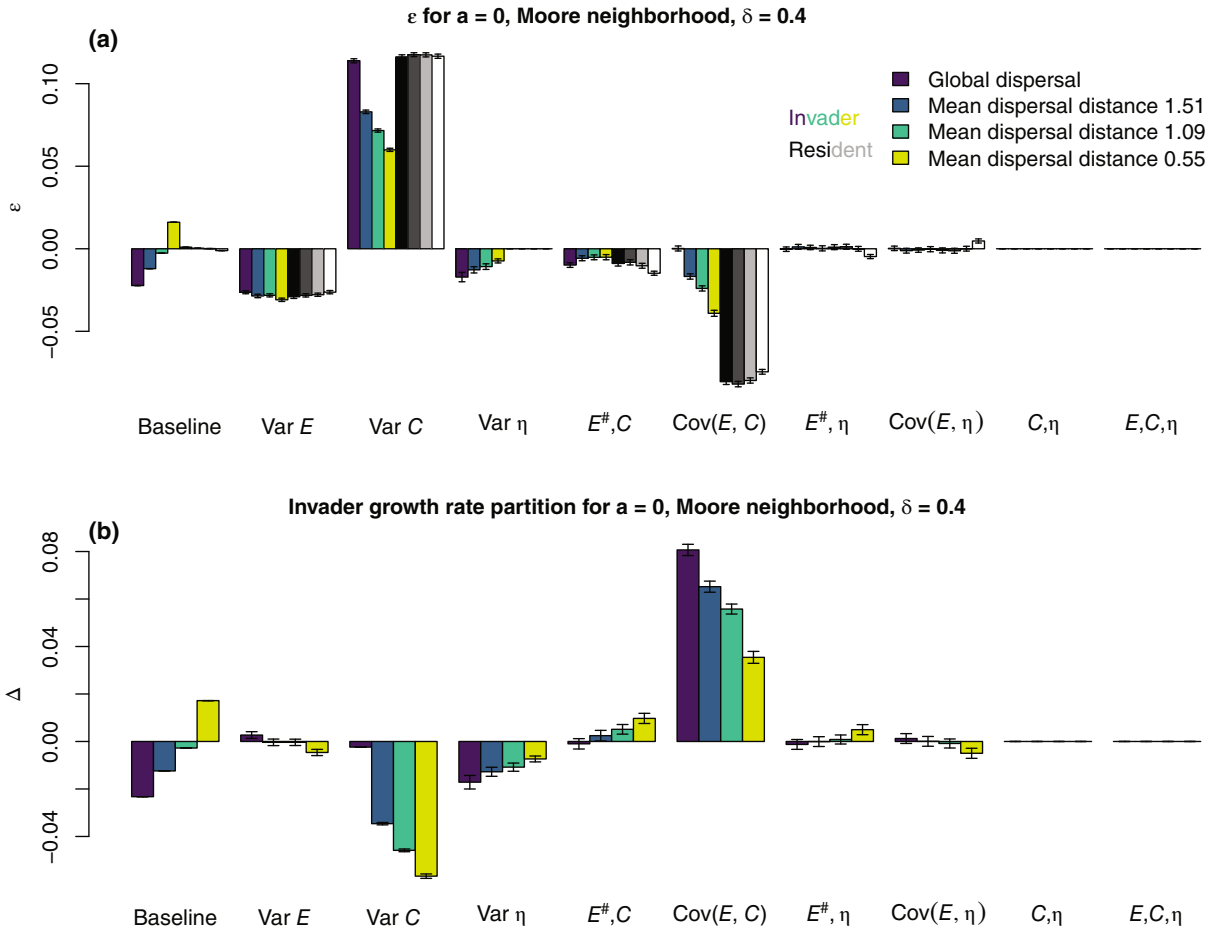

FIGURE 4 Barplot of partitions for the two-species lattice lottery model with Moore competition neighborhood and death rate $\delta = 0.4$. (a) $\bar{\varepsilon}$ partition for invader and resident. (b) Δ partition, that is, partition of invader growth rate into coexistence mechanisms. Lighter colors represent shorter-range dispersal, which produces more invader clustering. The mean dispersal distances for nonglobal dispersal correspond to α values 0.25, 0.5, and 1 in the dispersal matrix, Equation (10). At $\alpha = 0.25$, dispersal distance $d = 4$ (the maximum possible with nonglobal dispersal) is $e^{-1} \approx 37\%$ as likely as distance $d = 0$. Other parameter values: $M = 50$, $T = 500$, $K = 50$, $R = 20$, $V = 50$, $N_{\min} = 1$, $N_{\max} = 120$, $G_{\min} = 10$, $G_{\max} = 40$, $\mu_1 = 0.5$, $\mu_2 = 0.45$, $\sigma_1 = \sigma_2 = 0.6$, $\rho = -0.75$. Figure generated by plotDeltasVsAlpha2.R using simulation results generated by latticePartitionLoops.R and scripts that it sources using R version 4.1.1.

AnovaAnalyses.R). Variation in C directly benefits both invader and resident—this is inevitable because $1/C$ is a concave-up function of C—but with more clumping the direct benefit to the invader goes down (Figure 4a). As a result, the net effect of variation in C on invader growth rate goes from positive to negative with increased clumping in Figure 6. At the same time, for any given dispersal distance (color), increasing adult competition (going from $\circ$ to $\times$) increases ΔC. Variation in C directly benefits both invader and resident—this is inevitable because $1/C$ is a concave-up function of C—but with more clumping the direct benefit to the invader goes down (Figure 4a). This reduction is due to reduced variance in C. Increased clumping decreases mean competition (as shown by the increase in the baseline invader growth rate $\bar{\varepsilon}_0$), which would by itself instead increase the direct benefit of variation in C.

Plotting $\Delta\eta$ versus larval invader fraction (Figure 7), we confirm the finding of Hart et al. (2016) that demographic stochasticity reduces the invader growth rate by only a small amount. The average larval invasion fraction, mortality (δ), and their interaction explain 93% of the variance in $\Delta\eta$ (accounting for 31%, 59%, and 4%, respectively, of the total sum of squares). As discussed earlier, larval dispersal distance is the prime determinant of average larval invader fraction and, hence, a major determinant of $\Delta\eta$, but for a given dispersal distance, increasing adult competition increases the average larval invader fraction and, thus, reduces the magnitude of $\Delta\eta$. Demographic stochasticity causes the finite growth rate $\lambda = N_{t+1}/N_t$ to fluctuate and therefore decreases the long-run growth rate $\mathbb{E}[r] = \mathbb{E}[\log\lambda]$, since the log function is concave-down. Because the invader experiences greater

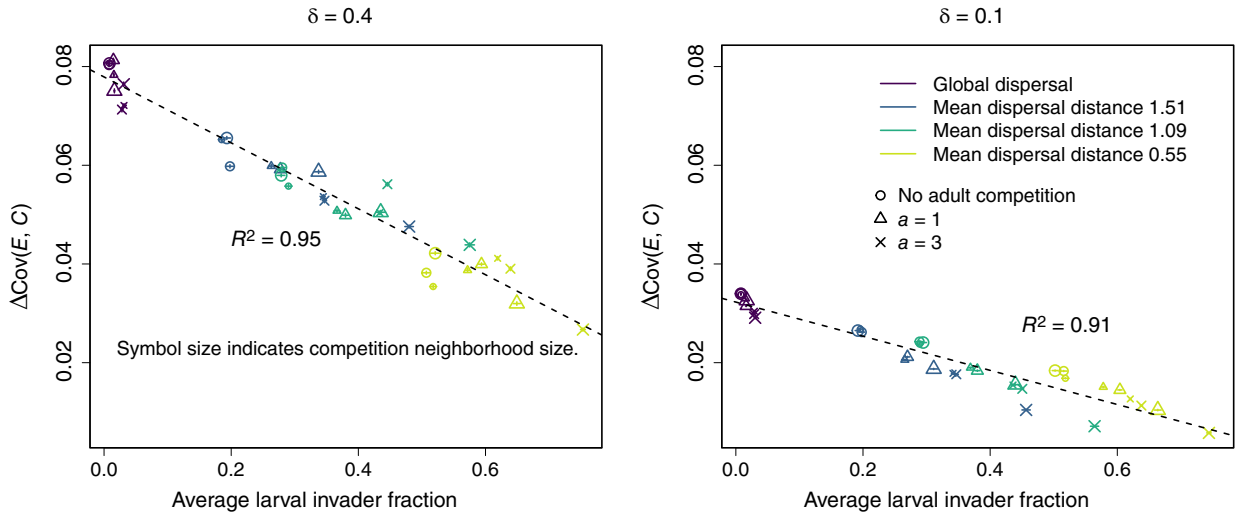

FIGURE 5 ΔCov(*E*,*C*) as a function of average larval invader fraction. ΔCov(*E*,*C*) is largely determined by average larval invader fraction and by the mortality rate δ. Lighter colors are for shorter-range dispersal. Size of the competition neighborhood is indicated by symbol size. The smallest points are for a Moore competition neighborhood, medium-sized points are for the Moore2 competition neighborhood, and the largest points are for global competition. Figure generated by plotDeltasVsLarvalInvFrac2.R using simulation results generated by latticePartitionLoops.R and scripts that it sources, using R version 4.1.1.

demographic stochasticity than the resident, demographic stochasticity suppresses invader growth more than resident growth, and Δη is negative. Though the effect of demographic stochasticity is small, it can be enough to change a barely successful invasion into a failed invasion; this happened in a number of our runs without adult competition ($a = 0$).

Why is Δη smallest when invaders are most clumped (Figure 7)? When invaders are highly clumped, there is little uncertainty about which species will win each vacant site because most vacant sites are either far from an invader clump or inside one. As a result, λ fluctuates less when the invaders become more clumped (Figure 8), invader growth rate is less suppressed, and Δη shrinks in magnitude.

So far, we have always assumed that invader and resident have the same larval dispersal distance. When those can differ, Figure 9 shows that average larval invader fraction is driven primarily by invader dispersal distance (i.e., lighter color symbols are to the right of darker symbols). An ANOVA analysis confirms that invader dispersal distance is the dominant factor, explaining 81% of the variance in average larval invader fraction, with resident dispersal distance contributing an additional 5% (within colors, circles and triangles are to the left of crosses and diamonds in Figure 9).

None of these findings is particularly surprising. What is most important is illustrating how the methodology we have introduced makes it possible to quantitatively partition the invasion growth rate into contributions from different mechanisms for spatial models with discrete individuals. As we review in the *Discussion* section, many questions remain about coexistence that the lattice lottery model does not address, but the tools to tackle those questions are now available.

PARTITION BASED ON LIFE-HISTORY DIFFERENCES

We turn now to a completely different coexistence mechanism, eliminating the recruitment fluctuations that are essential for coexistence in the lottery model. Instead, we allow the species to differ in life-history parameters μ (log of per-capita fecundity), δ (per-capita adult mortality), and α (dispersal range parameter). The spatial lottery model also allows fluctuation-independent coexistence in a constant environment based on these life-history differences. Shmida and Ellner (1984) showed this in a spatially implicit mean-field version of the model with a "top hat" dispersal kernel (i.e., some larvae remain in their natal site, while the rest disperse uniformly across all sites). Guided by the coexistence conditions for that model (their equation 8), we confirmed that the same kind of behavior occurs in our model: Coexistence in a constant environment (i.e., the only stochasticity in the model is the demographic stochasticity) can occur as a result of a large difference in per-capita fecundity, balanced by a large difference in per-capita survival probability (Figure 10a). Dispersal differences are not needed for coexistence. The survival–fecundity trade-off is analogous to the competition–colonization trade-off: One species is better at holding onto sites (by surviving), the

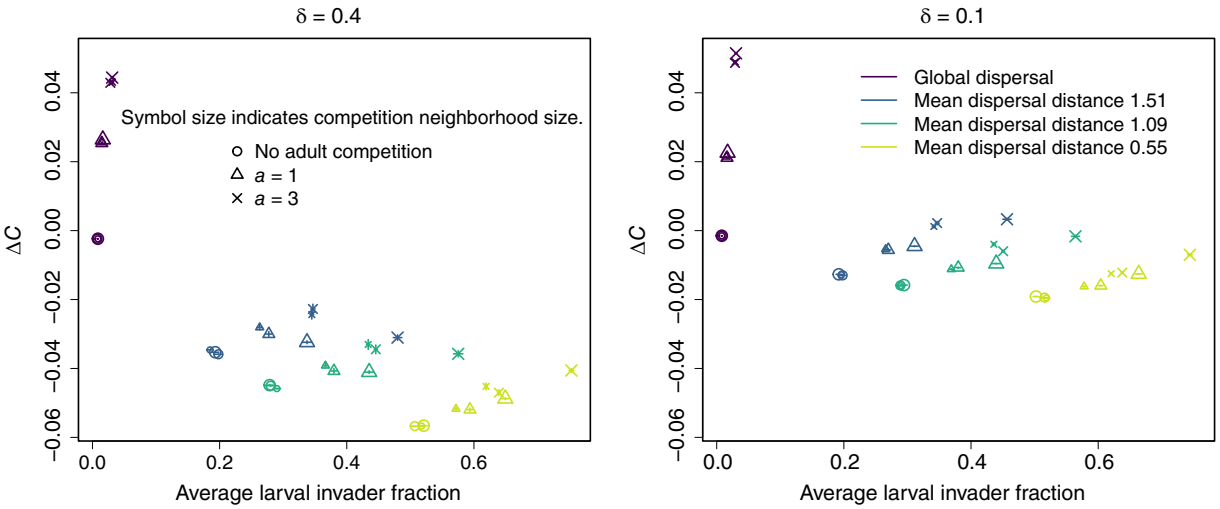

FIGURE 6 ΔC as a function of average larval invader fraction. Lighter colors are for shorter-range dispersal. In addition to the colors and symbols identified in the legend, the smallest size points are for a Moore competition neighborhood, the medium-sized points are for the Moore2 competition neighborhood, and the largest points are for global competition. Figure generated by plotDeltasVsLarvalInvFrac2.R using simulation results generated by latticePartitionLoops.R and scripts that it sources, using R version 4.1.1.

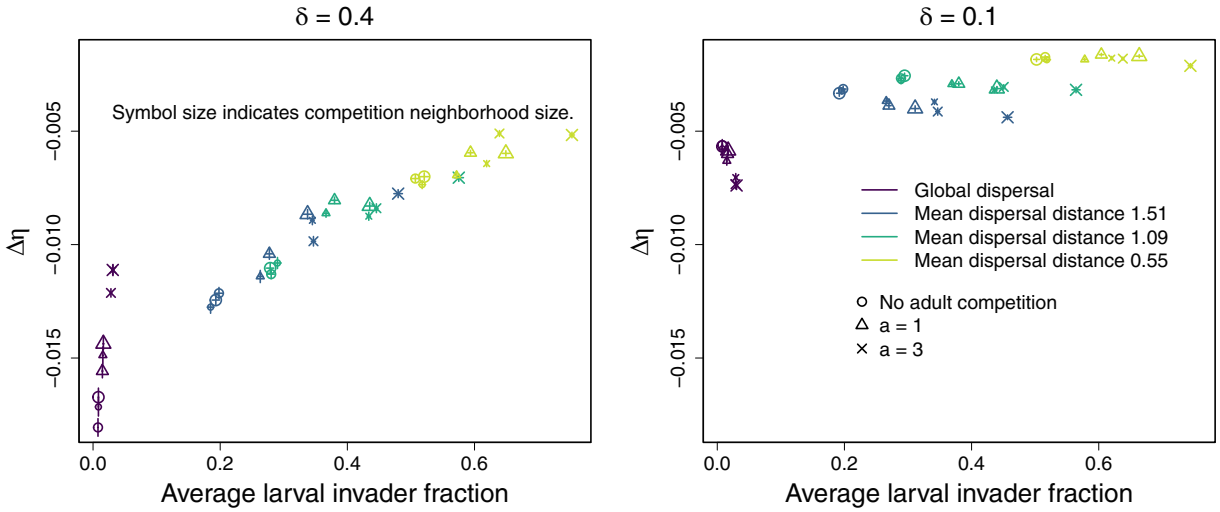

FIGURE 7 $\Delta\eta$ as a function of average larval invader fraction. Lighter colors are for shorter-range dispersal. In addition to the colors and symbols identified in the legend, the smallest size points are for a Moore competition neighborhood, the medium-sized points are for the Moore2 competition neighborhood, and the largest points are for global competition. Figure generated by plotDeltasVsLarvalInvFrac2.R, using simulation results generated by latticePartitionLoops.R and scripts that it sources, using R version 4.1.1.

other is better at taking open sites (by producing more larvae).

In this section, we explain and demonstrate how to partition invasion growth rates into contributions from the three life-history differences between the two competing species. This is an example of a "T decomposition" as defined by Ellner et al. (2019).

The three counterfactuals used in the partitioning are $\overline{\delta}$, in which both species have per-capita mortality rate $\delta = (\delta_1 + \delta_2)/2$; $\overline{\beta}$, in which both species have per-capita fecundity $\log\beta = (\log\beta_1 + \log\beta_2)/2$; and $\overline{\alpha}$, in which both species have $\alpha = (\alpha_1 + \alpha_2)/2$. As usual, these are applied individually and in all possible two- and three-way combinations to create the counterfactual scenarios used in the partitioning. Because we are interested in trait effects, demographic stochasticity is not included as a factor in the decomposition. The calculations, detailed in Appendix S1: Section S5, are very similar to those for the partition based on fluctuation-dependent mechanisms.

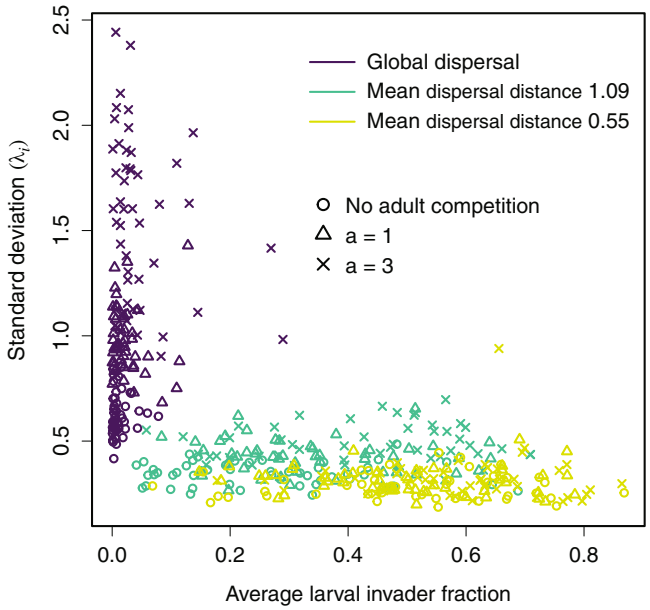

FIGURE 8 Standard deviation (λ_i) as a function of average larval invader fraction. Adult competition used the Moore neighborhood. Figure generated by plotVarLambdaVsLarvalInvFrac2.R using data generated by calcVarLambdaVsLarvalInvFrac.R and scripts that it sources using R version 4.0.2.

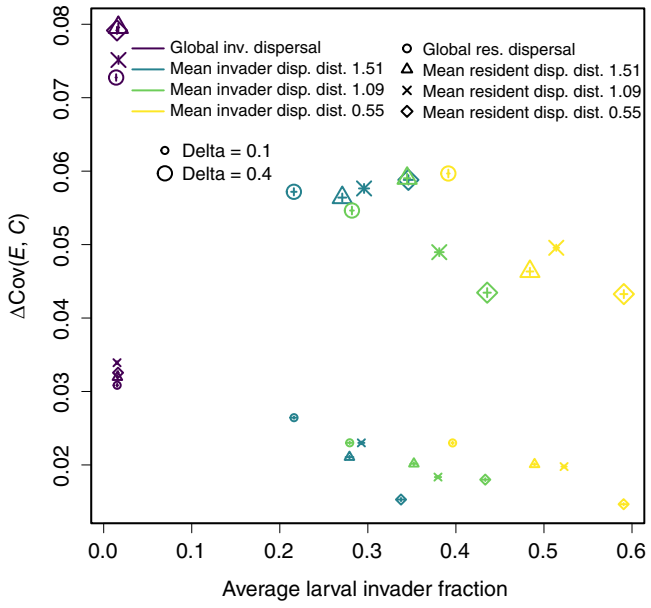

FIGURE 9 ΔCov(E, C) as a function of average larval invader fraction for independently varying resident and invader dispersal distances. Adult competition used the Moore2 neighborhood, with intensity $a = 1$. Figure generated by plotDeltasVsLarvalInvFracTwoAlphas.R using simulation results generated by latticePartitionLoops-twoD.R and scripts that it sources using R version 4.0.2. Parameter values (besides those labeled in the figure) are the same as in Appendix S1: Figure S5.

Trait differences in fecundity and survival—but not dispersal—contribute to coexistence, but their interactions are minimal (Figure 10b,c). Species 2 as invader gains from its higher fecundity slightly more than it loses due to its higher mortality—the reverse being true for Species 1 as invader. Species 1 is better at holding sites ($\delta_1 \ll \delta_2$), whereas the invader is better at claiming empty sites because of its much higher fecundity. Each species, as resident, creates a biotic environment where the other species has a slight advantage.

Changes in trait values largely affect the invader population growth rate, not the resident (Figure 10b). That is a consequence of the resident's ubiquity: It cannot increase much in our model because it already occupies most sites, and it cannot decrease much because most sites are so far from any invader that the resident always reclaims them if the occupant dies. Note that our previous partition based on fluctuation-dependent mechanisms includes counterfactuals where the resident population can change substantially in one time step—for example, removing E, C covariance allows the resident population to increase significantly in years when E is high but C is nonetheless low for the resident. Hence some counterfactuals have large effects on expected resident population growth in Figure 4a, but none do in Figure 10b.

DISCUSSION

Here we have shown quite generally how to estimate contributions to coexistence for discrete and spatial models by partitioning invader growth rates. This method can be used to partition among any variables or mechanisms, not just the classic environment–competition partition. As a demonstration, we applied our method to the lattice lottery model. Our first partition was according to the contributions of variable environment, variable competition, and demographic stochasticity. Our second example examined a constant-environment lattice model in which a fecundity–survival trade-off maintains coexistence and partitioned the contributions to coexistence from the differences in fecundity, mortality, and dispersal.

Using the lattice lottery model, we found that the effects of environment–competition covariance (E, C covariance) and variable competition on coexistence are strongly affected by invader clumping, which is in turn driven mostly by the range of invader dispersal, though invaders also become slightly more clumped as adult competition becomes stronger. Recall that in the classical lottery model, E, C covariance benefits the invader indirectly by harming

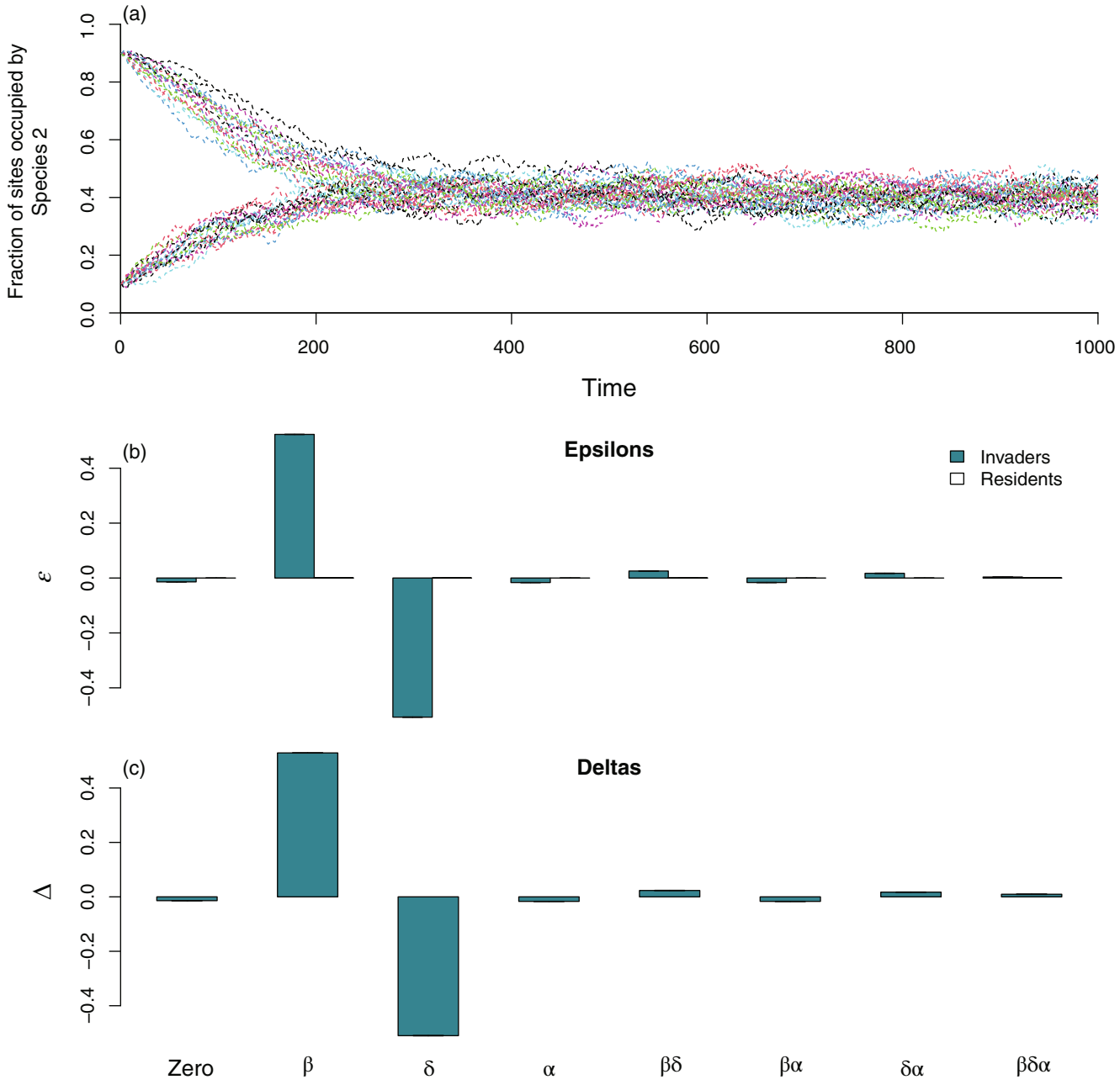

FIGURE 10 Partition for fluctuation-independent coexistence based on life-history differences between two species. (a) Simulations of lattice lottery model on a 50 × 50 lattice with parameter values $\mu_1 = \log\beta_1 = 1, \mu_2 = \log\beta_2 = 1 + \log(3) \approx 2.1, \delta_1 = 0.2, \delta_2 = 0.8, \alpha_1 = 0.1, \alpha_2 = 0.3$. Although all parameters (in particular fecundity) are constant over time, population size fluctuates due to demographic stochasticity rather than converging to an equilibrium. (b, c) $\bar{\varepsilon}$ and Δ trait partitions of Species 2 invasion growth rate, direct effects only. Figure generated by scripts DeathFecundityTradeoffSimulate.R, survFecTradeoffPartitionDirectOnly.R, plotTraitDeltasDirect.R using R version 4.1.1.

the resident: because a good E entails a high C for the resident, the resident cannot benefit from years with potentially high recruitment. In contrast, the invader, with much lower E, C covariance, can "make hay while the sun shines." In our spatial lottery model, when invaders are more clumped, they compete with each other more intensely when rare, so they too become limited by their own E, C covariance. More invader clumping also means that variation in competition changes from helping the invader to harming it. More broadly, invader clumping is likely to weaken any coexistence mechanism that relies on the invader escaping competition from the resident, because invader clumping means that the resident is no longer the only source of competition.

Invader clumping need not be entirely detrimental to the invader. If we had used a model where the resident population density could vary from site to site or even leave gaps, then this would have opened up another way for the invader to avoid competition: by exploiting ephemeral areas of low resident density (Bolker & Pacala, 1999; Hassell et al., 1991), which can arise randomly or through endogenous spatial dynamics (e.g., Comins & Hassell, 1996; Durrett & Levin, 1997; Hassell et al., 1994). Alternatively, if we allowed more than one individual at a site and there were a founder effect, so that the invader could hold a site once it had won it, then again, invader clumping could boost the invader growth rate (Bolker & Pacala, 1999). These are examples of the general principle that short-range dispersal can allow a species to concentrate its population in areas where its local growth rate is high and thereby boosts its invasion growth rate (Snyder & Chesson, 2003). Nonetheless, once we consider the invader's competitive effect on itself, we expect that these coexistence mechanisms will be weakened.

Some theoretical studies have suggested that species clumping should enhance coexistence because it reduces contacts between an inferior competitor and a superior competitor, for example (Murrell et al., 2001). Chesson and Neuhauser (2002) pointed out that this is not correct if clusters are solid: though competition is indeed reduced inside a cluster of competitively inferior individuals, what determines whether a population increases or decreases is whether the cluster expands or contracts at its boundary, and boundary movement necessarily depends on between-species competition. Invader clusters in our model are not solid, so it is possible for a cluster to grow by filling in. However, this does not mean that invader clumping promotes coexistence. Rather, because the invader and resident find different times favorable, invader clumping means that an invader individual is more likely to have neighbors who also experience the current year as favorable, increasing competition.

We also confirmed the findings of Hart et al. (2016) that demographic stochasticity hurts the invader but that the effect size is very small. Turelli (1980), who examined the combined effects of demographic stochasticity and temporal environmental variation, also found that demographic stochasticity had a modest negative effect on coexistence, although temporal variation reduces rather than enables coexistence in that model. (To isolate the effect of demographic stochasticity in that paper, note that the finite growth rate in the absence of demographic stochasticity or temporal variation is given on p. 127 of that paper as $1 + r(1 - \gamma(\alpha))$—the invasion probabilities in Turelli's table 1 do decline steeply when the finite growth rate gets close to 1). Nonetheless, demographic stochasticity can turn a barely positive invader growth rate into a negative one, thereby preventing coexistence. We hypothesize that demographic stochasticity could

TABLE 1 Notation and definitions.

Notation	Formula or meaning
a_{qs}	Competitive effects of species s adults on species q adults
$\beta_q(t)$	Fecundity of species q at time t
$C_q(t)$	Competition experienced by species q at time t
$D_{x'\|x}$	Dispersal probability from site x to site x'
δ_q	Mortality rate of species q
Δ_k	Invader–resident comparison $\varepsilon_{ik} - \varepsilon_{rk}$
$E_q(t)$	Environment experienced by species q at time t
$E_q^{\sharp}(t)$	Temporally shuffled environments experienced by species q
$\varepsilon_{q,k}$	fANOVA contribution of effect k for species q
$\eta_q(t)$	Demographic stochasticity for species q at time t
$F_{q,x}(t)$	Number of larvae produced by a species q parent at site x at time t
$G_{\min}$, $G_{\max}$	Fleming–Viot algorithm generates "small" invader clusters with size between $G_{\min}$ and $G_{\max}$
K	Number of lattice configurations used in one-step-ahead model simulations
$N_q(t)$	Population size of species q at time t
$\mathcal{N}_x$	Set of sites that are neighbors of x for adult competition
r_q	Long-run growth rate of species q
R	Number of replicates per vacancy configuration in one-step-ahead model simulations
$\overline{R}_q(t)$	Expected number of species q recruits at time t
$\overline{S}_q(t)$	Expected number of surviving adults of species q at time t
V	Number of vacancy configurations per lattice configuration in one-step-ahead model simulations
χ_q	Population growth measure being partitioned, calculated here as $\overline{r}_q$
$y_{q,x}(t)$	Number of species q larvae landing in site x at time t
Z_x	Normalization constant for dispersal probability function $D_{x'\|x}$
z	Number of sites in adult competition neighborhood
$\bullet^{(r\|v,k)}$	Quantity $\bullet$ for replicate r conditional on vacancy configuration v and lattice configuration k, for example, $C_q^{(r\|v,k)}(t)$

Abbreviation: fANOVA, functional Analysis of Variance.

have stronger effects on coexistence in models where sites can remain unoccupied. Demographic stochasticity could then create localized extinctions that might qualitatively change dynamics, for example by creating transient openings that maintain a fugitive species.

The analysis by Lande (1998) predicted that demographic stochasticity would reduce an invader's growth rate most severely when its population size was smallest, but we have not observed that in our model (e.g., Appendix S1: Figure S2D does not show a dip in invader growth rate [average change in log N] as total invader population N approaches zero). But Lande's model differs from ours in several important ways: it is nonspatial, and it employs a diffusion approximation with continuous population size even for small populations. Lande (1998) also assumed that at low density the fates of invaders were independent. Because invaders are spatially clustered in our model, their fates are correlated even when invaders are rare: if one of my offspring gets a site, my neighbors' offspring do not.

We have only treated temporal environmental variation, but we plan to address fixed spatial variation and spatiotemporal variation soon. Spatial variation that is permanent or long-lasting can powerfully promote coexistence if it permits the invader population to concentrate in areas where growth rate is highest (either because of a favorable environment or low competition) (Snyder, 2008; Snyder & Chesson, 2003), a mechanism called growth-density covariance (Chesson, 2000a). We hypothesize that, once we have partitioning methods for discrete spatial models with spatially or spatiotemporally varying habitat quality, growth-density covariance will frequently prove to be a stronger coexistence mechanism than the spatial storage effect (a storage effect caused by environmental variation in space instead of time). This difference may be even greater with discrete individuals (relative to the cited previous results with continuous population density) if invader clumping reduces the spatial storage effect, analogously to our findings here about the temporal storage effect.

A more difficult goal is answering the question of what to partition. Some have argued that invasion growth rates are not an adequate guide to coexistence because they ignore demographic stochasticity and that we should really focus on something like expected time to extinction (Pande et al., 2020). Here we continue to partition invasion growth rates, for two reasons. First, the sign of the invasion growth rate distinguishes two different regimes (Ellner et al., 2020): If the invasion growth rate for a species is negative, then time to extinction is always short, whereas if all invasion growth rates are positive, then the mean time to extinction increases rapidly with community size (e.g., the total amount of space or resources that is available to individuals in the community). Thus, positive invasion growth rates are necessary for coexistence, and it is meaningful to ask which mechanisms or processes contribute to their being positive. Second, the existing conceptual framework for partitioning invasion growth rates is well developed and provides the basis for our extension here to discrete spatial populations. In particular, we know that a meaningful partitioning needs to account for each mechanism's effect on both the invader and the resident, because something that harms a resident species more than it harms the invader can promote coexistence just as much as something that benefits the invader directly. For invasion growth rates, these indirect benefits are accounted for by partitioning both invader and resident population growth rates, as we have demonstrated. At present, it is not known how to account for these indirect benefits when extinction time is used to quantify coexistence.

However, even with a decision to focus on invasion rates, it is not clear what definition of invasion rate is sensible in a spatial context—we need a measure that becomes independent of invader density (or nearly so) when the invader is sufficiently rare. In Appendix S1: Section S2 we briefly discuss why we think that $\mathbb{E}\log(N_{t+1}/N_t)$ is the best available measure in our model when the range of natal dispersal is not too narrow, but more work remains to be done.

We close with a plea for experimental studies that collect all of the data needed to apply our methods to real-world systems, including data on fixed spatial variation or spatiotemporal variation in habitat quality for different species. We now have the machinery to partition coexistence mechanisms in any spatial model, but we remain unable to estimate the strength of different coexistence mechanisms in real systems because we do not have fully parameterized models. The data requirements are daunting: Researchers will need measurements of demographic parameters and their variation in time and space, the strengths of interactions as a function of distance, and dispersal distributions. However, because we now have the theoretical machinery to take advantage of those data, whatever form the appropriate model may take, we believe that our best hope for understanding the relative importance of different coexistence mechanisms is for experimental ecologists to collect the necessary data and build fully parameterized data-driven models for the spatial and temporal dynamics of interacting species.

AUTHOR CONTRIBUTIONS

All authors contributed to conceiving the project, discussed all aspects of the research, and helped write and revise the paper. Stephen P. Ellner and Robin E. Snyder did most of the coding and wrote most of the first draft.

ACKNOWLEDGMENTS

This research was supported by US National Science Foundation Grants DEB-1933497 (Stephen P. Ellner and Giles Hooker), DEB-1933612 (Robin E. Snyder), and DEB-1933561 (Peter B. Adler). We learned about the Fleming–Viot algorithm from Sebastian Schreiber. We thank Megan Greischar, Christina Hernández, Tim Lambert, Jonathan Levine, Chris Myers, Wee Hao Ng, Anna Poulton, Gregor-Fausto Siegmund, Jürg Spaak, and our reviewers (György Barabás and one anonymous) for very helpful comments on the manuscript.

CONFLICT OF INTEREST

The authors declare no conflict of interest.

DATA AVAILABILITY STATEMENT

No data were collected for this study or used in this study. Novel code (in the form of R scripts) supporting all results are in a publicly available archive on Figshare, https://doi.org/10.6084/m9.figshare.17113967.v3 (Ellner et al., 2022). The caption for each figure in the paper that contains results identifies exactly which script(s) generated the figure.

ORCID

Stephen P. Ellner https://orcid.org/0000-0002-8351-9734
Robin E. Snyder https://orcid.org/0000-0002-6111-0284
Peter B. Adler https://orcid.org/0000-0002-4216-4009

REFERENCES

Allstadt, A., T. Caraco, and G. Korniss. 2007. "Ecological Invasion: Spatial Clustering and the Critical Radius." *Evolutionary Ecology Research* 9: 375–94.

Asselah, A., P. A. Ferrari, and P. Groisman. 2011. "Quasistationary Distributions and Fleming-Viot Processes in Finite Spaces." *Journal of Applied Probability* 48: 322–32.

Benaim, M., and S. J. Schreiber. 2019. "Persistence and Extinction for Stochastic Ecological Models with Internal and External Variables." *Journal of Mathematical Biology* 79: 393–431.

Bessonov, M., and R. Durrett. 2017. "Phase Transitions for a Planar Quadratic Contact Process." *Advances in Applied Mathematics* 87: 82–107.

Bolker, B. M., and S. W. Pacala. 1999. "Spatial Moment Equations for Plant Competition: Understanding Spatial Strategies and the Advantages of Short Dispersal." *The American Naturalist* 153: 575–602.

Chan, B., and R. Durrett. 2006. "A New Coexistence Result for Competing Contact Processes." *Annals of Applied Probability* 16: 1155–65.

Chesson, P. 1982. "The Stabilizing Effect of a Random Environment." *Journal of Mathematical Biology* 15: 1–36.

Chesson, P. 1994. "Multispecies Competition in Variable Environments." *Theoretical Population Biology* 45: 227–76.

Chesson, P. 2000a. "General Theory of Competitive Coexistence in Spatially-Varying Environments." *Theoretical Population Biology* 58: 211–37.

Chesson, P. 2000b. "Mechanisms of Maintenance of Species Diversity." *Annual Review of Ecology and Systematics* 31: 343–66.

Chesson, P., and S. Ellner. 1989. "Invasibility and Stochastic Persistence in Monotonic Competition Models." *Journal of Mathematical Biology* 27: 117–38.

Chesson, P., and C. Neuhauser. 2002. "Intraspecific Aggregation and Species Coexistence." *Trends in Ecology and Evolution* 17: 210–1.

Chesson, P., and R. Warner. 1981. "Environmental Variability Promotes Coexistence in Lottery Competitive Systems." *American Naturalist* 117: 923–43.

Comins, H. N., and M. P. Hassell. 1996. "Persistence of Multispecies Host-Parasitoid Interactions in Spatially Distributed Models with Local Dispersal." *Journal of Theoretical Biology* 183: 19–28.

Cox, J., and R. Durrett. 1988. "Limit Theorems for the Spread of Epidemics and Forest Fires." *Stochastic Processes and their Applications* 30: 171–91.

Durrett, R. 1988. "Crabgrass, Measles, and Gypsy Moth: An Introduction to Modern Probability." *Bulletin (New Series) of the American Mathematical Society* 18: 117–43.

Durrett, R. 2002. "Mutual Invadability Implies Coexistence in Spatial Models." *Memoirs of the American Mathematical Society* 156: 740.

Durrett, R. 2009. "Coexistence in Stochastic Spatial Models." *Annals of Applied Probability* 19: 477–96.

Durrett, R., and S. Levin. 1994. "The Importance of Being Discrete (and Spatial)." *Theoretical Population Biology* 46: 363–94.

Durrett, R., and S. Levin. 1997. "Allelopathy in Spatially Distributed Populations." *Journal of Theoretical Biology* 185: 165–71.

Ellner, S., R. E. Snyder, G. Hooker, and P. B. Adler. 2022. "R Scripts for the Paper, Toward a "Modern Coexistence Theory" for the Discrete and Spatial, by Ellner, Snyder, Adler and Hooker, Ecological Monographs." Figshare. https://doi.org/10.6084/m9.figshare.17113967.v3.

Ellner, S. P., R. E. Snyder, and P. B. Adler. 2016. "How to Quantify the Temporal Storage Effect Using Simulations Instead of Math." *Ecology Letters* 19: 1333–42.

Ellner, S. P., R. E. Snyder, P. B. Adler, and G. Hooker. 2019. "An Expanded Modern Coexistence Theory for Empirical Applications." *Ecology Letters* 22: 3–18.

Ellner, S. P., R. E. Snyder, P. B. Adler, G. Hooker, and S. J. Schreiber. 2020. "Technical Comment on Pande et al. (2020): Why Invasion Analysis Is Important for Understanding Coexistence." *Ecology Letters* 23: 1721–4.

Gandhi, A., S. Levin, and S. Orszag. 1999. "Nucleation and Relaxation from Meta-Stability in Spatial Ecological Models." *Journal of Theoretical Biology* 200: 121–46.

Groisman, P., and M. Jonckheere. 2013. "Simulation of Quasi-Stationary Distributions on Countable Spaces." *Markov Processes and Related Fields* 19: 521–42.

Hart, S. P., S. J. Schreiber, and J. M. Levine. 2016. "How Variation between Individuals Affects Species Coexistence." *Ecology Letters* 19: 825–38.

Hassell, M., H. Comins, and R. May. 1991. "Spatial Structure and Chaos in Insect Population Dynamics." *Nature (London)* 353: 255–8.

Hassell, M. P., H. N. Comins, and R. M. May. 1994. "Species Coexistence and Self-Organizing Spatial Dynamics." *Nature (London)* 370: 290–2.

Hening, A., and D. H. Nguyen. 2018. "Coexistence and Extinction for Stochastic Kolmogorov Systems." *Annals of Applied Probability* 28: 1893–942.

Hening, A., and D. H. Nguyen. 2020. "The Competitive Exclusion Principle in Stochastic Environments." *Journal of Mathematical Biology* 80: 1323–51.

Hening, A., D. H. Nguyen, and P. Chesson. 2021. "A General Theory of Coexistence and Extinction for Stochastic Ecological Communities." *Journal of Mathematical Biology* 82: 56.

Hooker, G. 2007. "Generalized Functional ANOVA Diagnostics for High Dimensional Functions of Dependent Variables." *Journal of Computational and Graphical Statistics* 16: 709–32.

Korniss, G., and T. Caraco. 2005. "Spatial Dynamics of Invasion: The Geometry of Introduced Species." *Journal of Theoretical Biology* 233: 137–50.

Kot, M. 2003. "Do Invading Organisms Do the Wave?" *Canadian Applied Mathematics Quarterly* 10: 139–70.

Kot, M., J. Medlock, and T. Reluga. 2006. "Stochasticity, Invasions, and Branching Random Walks." *Theoretical Population Biology* 66: 175–84.

Lande, R. 1998. "Demographic Stochasticity and Allee Effect on a Scale with Isotropic Noise." *Oikos* 83: 353–8.

Lewis, M. 2000. "Spread Rate for a Nonlinear Stochastic Invasion." *Journal of Mathematical Biology* 41: 430–54.

Lutscher, F. 2019. *Integrodifference Equations in Spatial Ecology*. Cham, Switzerland: Springer Nature, Switzerland AG.

Murrell, D. J., D. W. Purves, and R. Law. 2001. "Uniting Pattern and Process in Plant Ecology." *Trends in Ecology and Evolution* 16: 529–30.

O'Malley, L., J. Basham, J. A. Yasi, G. Korniss, A. Allstadt, and T. Caraco. 2006. "Invasive Advance of an Advantageous Mutation: Nucleation Theory." *Theoretical Population Biology* 70: 464–78.

O'Malley, L., G. Korniss, and T. Caraco. 2009. "Ecological Invasion, Roughened Fronts, and a Competitor's Extreme Advance: Integrating Stochastic Spatial-Growth Models." *Bulletin of Mathematical Biology* 71: 1160–88.

Pande, J., T. Fung, R. Chisholm, and N. M. Shnerb. 2020. "Mean Growth Rate When Rare Is Not a Reliable Metric for Persistence of Species." *Ecology Letters* 23: 274–82.

Reluga, T. 2016. "The Importance of Being Atomic: Ecological Invasions as Random Walks Instead of Waves." *Theoretical Population Biology* 112: 157–69.

Roth, G., and S. J. Schreiber. 2014. "Persistence in Fluctuating Environments for Interacting Structured Populations." *Journal of Mathematical Biology* 69: 1267–317.

Schreiber, S. J., M. Benaim, and K. A. S. Atchade. 2011. "Persistence in Fluctuating Environments." *Journal of Mathematical Biology* 62: 655–83.

Shmida, A., and S. Ellner. 1984. "Coexistence of Plant Species with Similar Niches." *Plant Ecology* 58: 29–55.

Snyder, R. E. 2003. "How Demographic Stochasticity Can Slow Biological Invasions." *Ecology* 6: 301–9.

Snyder, R. E. 2008. "When Does Environmental Variation Most Influence Species Coexistence?" *Theoretical Ecology* 1: 129–39.

Snyder, R. E., E. T. Borer, and P. Chesson. 2005. "Examining the Relative Importance of Spatial and Nonspatial Coexistence Mechanisms." *The American Naturalist* 166: E75–94.

Snyder, R. E., and P. Chesson. 2003. "Local Dispersal Can Facilitate Coexistence in the Presence of Permanent Spatial Heterogeneity." *Ecology Letters* 6: 301–9.

Snyder, R. E., and P. Chesson. 2004. "How the Spatial Scales of Dispersal, Competition, and Environmental Heterogeneity Interact to Affect Coexistence." *The American Naturalist* 164: 633–50.

Turelli, M. 1980. "Niche Overlap and Invasion of Competitors in Random Environments II. The Effects of Demographic Stochasticity." In *Biological Growth and Spread, Lecture Notes in Biomathematics*, Vol 38, edited by W. J. Ager, H. Rost, and P. Tautu, 119–29. Berlin, Germany: Springer-Verlag.

Usinowicz, J. 2015. "Limited Dispersal Drives Clustering and Reduces Coexistence by the Storage Effect." *American Naturalist* 186: 634–48.

SUPPORTING INFORMATION

Additional supporting information can be found online in the Supporting Information section at the end of this article.

How to cite this article: Ellner, Stephen P., Robin E. Snyder, Peter B. Adler, and Giles Hooker. 2022. "Toward a "Modern Coexistence Theory" for the Discrete and Spatial." *Ecological Monographs* 92(4): e1548. https://doi.org/10.1002/ecm.1548

Appendix S1

Stephen P. Ellner, Robin E. Snyder, Peter B. Adler, and Giles Hooker, Toward a "Modern Coexistence Theory" for the Discrete and Spatial, *Ecological Monographs*.

Section S1 Formulas for calculating competition C_q

C_q can be calculated as follows. Conditional on the environments $\beta_s(t)$ for all species, the expected number of new species q recruits at $(t+1)$ is the sum over all sites of the probability that the site becomes vacant, times the probability that species q wins the lottery for the site. Let $n_{s,x}(t)$ be 1 at sites occupied by a species s adult, zero elsewhere. The probability that site x becomes vacant is then

$$V_x(t) = \sum_s \delta_s n_{s,x}(t). \qquad \text{(Eq. S1)}$$

The expected number of species q new recruits $\bar{R}_q(t+1)$ is then

$$\bar{R}_q(t+1) = \sum_x V_x(t) \frac{y_{q,x}(t)}{\sum_s y_{s,x}(t)}. \qquad \text{(Eq. S2)}$$

We define C so that $\bar{R} = NE/C$, thus

$$C_q(t) = \frac{\beta_q(t) N_q(t)}{\bar{R}_q(t+1)}. \qquad \text{(Eq. S3)}$$

A potential difficulty with (Eq. S3) is that $\bar{R}_q(t+1) = 0$ whenever $\beta_q(t) = 0$. To handle that situation we define $C_q(t)$ as the limiting value of the definition above as $\beta_q(t) \to 0$. That is really the only sensible definition, because it is the only way to make C_q a continuous function of β_q. For example if $\beta_q(t)$ has a point-mass at zero and otherwise is lognormally distributed, we want the value of C_q for $\beta_q = 0$ to be very close to the value for $\beta_q = 0.001$.

The limit as $\beta_q(t) \to 0$ is as follows. Note that $y_{q,x}(t) = \beta_q(t) y^{(1)}_{q,x}(t)$, where $y^{(1)}_{q,x}(t)$ is the value that $y_{q,x}(t)$ would take if $\beta_q(t)$ has the value 1 in eqns. (11) and (12). Consequently

$$\bar{R}_q(t+1) = \beta_q(t) \sum_x V_x(t) \frac{y^{(1)}_{q,x}(t)}{\beta_q(t) y^{(1)}_{q,x}(t) + \sum_{s \neq q} y_{s,x}(t)}. \qquad \text{(Eq. S4)}$$

So as $\beta_q(t) \to 0$,

$$\frac{1}{C_q(t)} = \frac{\bar{R}_q(t+1)}{N_q(t)\beta_q(t)} \to \frac{1}{N_q(t)} \sum_x V_x(t) \frac{y^{(1)}_{q,x}(t)}{\sum_{s \neq q} y_{s,x}(t)}. \quad \text{(Eq. S5)}$$

Section S2 Defining invader growth rate for a discrete, spatial system.

Analysis of coexistence through invasion growth rates is based on the premise that an invading population grows exponentially so long as it is so rare that it does not compete with itself. This means that the change in log$N$ over one time step (or the expected change, in a stochastic environment model) is independent of N over the range of population sizes N for which the invader does not compete with itself. This is true even in spatial models with continuous population size, for example integrodifference equation models, where the long-term population behavior is a traveling wave with constant velocity implying that the rate of change in N (in one dimension) or $\sqrt{N}$ (in two dimensions) is independent of N when N is large.

But with discrete individuals in a spatial system, such as the lattice lottery model that we consider here, if offspring tend to be near their parents due to limited natal dispersal or mobility, an invader will typically start to compete with itself after just one or two time steps when it is still very rare. Even if an individual and its parent do not compete directly (e.g., they do not increase each other's mortality, or decrease each other's production of seeds or larvae), the natal dispersal range for their offspring necessarily has considerable overlap resulting in competition at the offspring recruitment stage. Shorter-range dispersal and direct competition between adults will result in competition becoming important at smaller invader population sizes.

Simulation results in Fig. S1 confirm that in our lattice lottery model, even a rare invader ($N = 10$ to 40) is sufficiently clustered that the Moore2 neighborhood of a typical invader individual (i.e., the 5×5 square of lattice cells centered on the individual) contains several other invader individuals. So even when adult competition is absent ($a = 0$) or limited to nearest neighbors, the larvae of a typical invader individual will be competing with larvae from other invaders.

But competition at low densities does not rule out exponential or approximately exponential population growth if the intensity of competition experienced by a typical individual does not vary with N. In that case, the one-step change in log$N$ would be (approximately) independent of initial population. Alternatively, if an initial small cluster of invaders quickly reaches its local "carrying capacity" within the

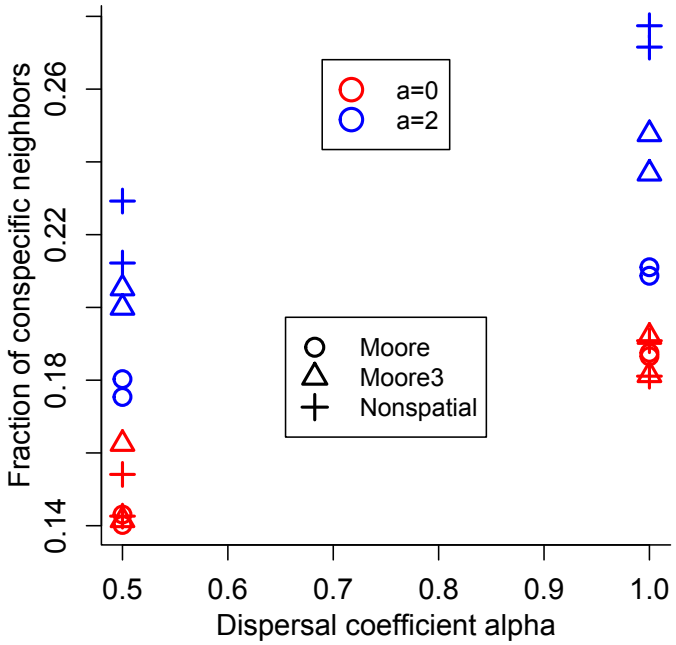

Figure S1: Average fraction of conspecific individuals in the Moore2 neighborhood of an invader individual in the lattice lottery model. Simulations of the lattice lottery model were run on a 60×60 lattice, initialized with the invader as a 2×2 cluster of individuals and all other sites occupied by the resident. The invader population was re-initialized whenever the total population fell to 0 or exceeded 100, so that the state at $T = 1000$ should represent a typical state during the initial spread of the invader. Parameter values were $a = 0$ or 2, $\alpha = 0.5$ or 1, $\delta = 0.1$ or 0.4, and adult competition neighborhood either Moore, Moore3, or global competition. Parameters $\mu_1 = 0.5, \mu_2 = 0.45$ (with species 2 the invader), $\sigma_1 = \sigma_2 = 0.6, \rho = -0.75$ were the same for all runs. For each parameter combination 400 parallel simulations were run, and the fraction of invader neighbors was computed for all final population states with total invader population $10 \leq N \leq 40$, up to a maximum of 100 such states. Figure produced by script `ClusterInvaderCompetition.R` using R version 4.1.1.

region it occupies, we might see population growth characteristic of a traveling wave in two dimensions, with the one-step change in $\sqrt{N}$ roughly independent of initial population.

To see if either of these occurs in our model, we conducted a series of model simulations as described in section *Generating a sample of lattice configurations with small invader clusters*, at a series of model parameter settings. For each parameter combination (described below) we did $K = 250$ parallel simulations on a 50×50 lattice and computed the population change for 100 replicate one-step-ahead simulations from lattice configurations at $T = 500$ with invader population N between 10 and 40. Figure

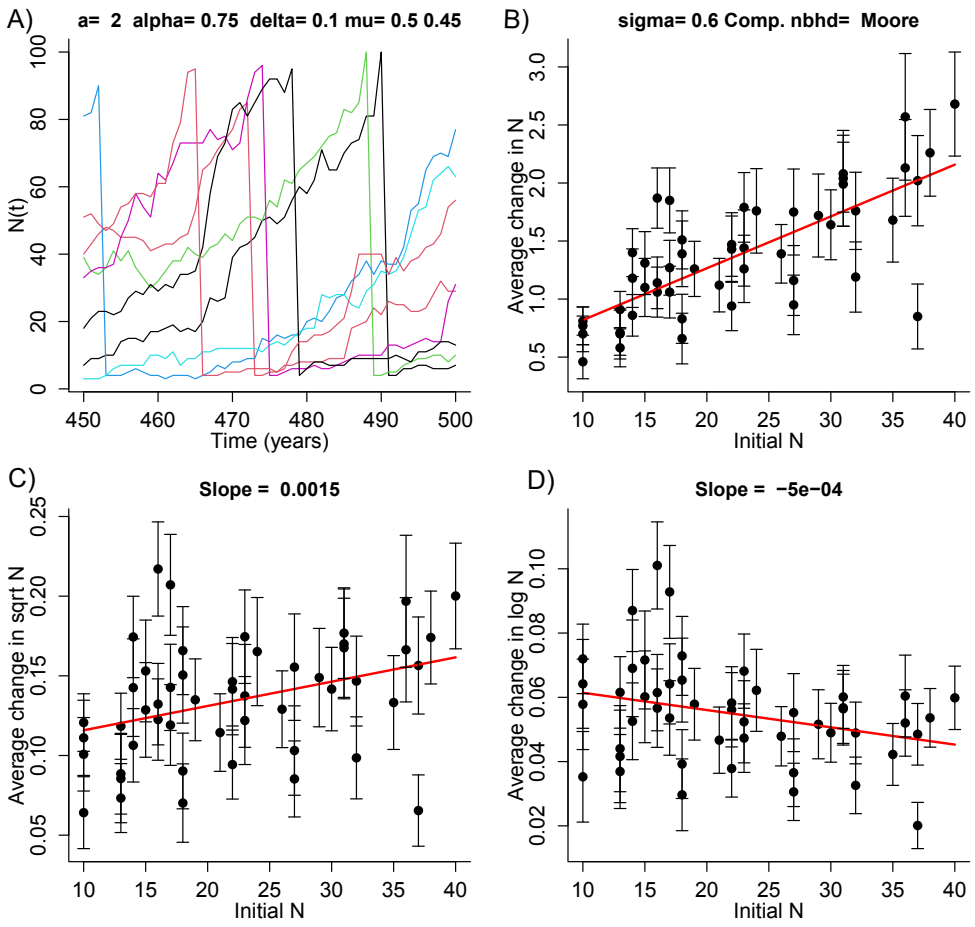

Figure S2: An example of simulation results on the relationship between invader population N and invader population growth rate. A) a sample of simulation trajectories, showing re-initializations. B) Plot of one-step-ahead change in N versus N. Plotted points are the mean ($\pm$ one standard error) of the change in N across 100 replicate one-step-ahead simulations from a lattice configuration at time $T = 500$. C) Plot of the change in $\sqrt{N}$. The red curve is a regression line fitted to all one-step-ahead changes. D) Plot of the change in $\log N$, as in C). Figure produced by script `CompareClusterMetrics-loops.R` using R version 4.1.1.

S2 illustrates a typical outcome when the invader increases robustly when rare (panels A and B). The one-step change in $\sqrt{N}$ increases with initial population size, representing an accelerating wave. The one-step change in $\log N$ decreases slightly with population size (note the difference in y-axis scale between panels C and D). This corresponds to roughly exponential growth, with the growth rate gradually slowing as the population grows due to gradually increasing impacts of density dependence.

As model parameters are varied, there is a tight relationship between the average one-step change in $\log N$ or $\sqrt{N}$ for $10 \leq N \leq 40$ and the slope of the fitted regression line (Fig. S3A, B). In both cases the magnitude of the slope is about 1% of the average. In both cases, the highest averages and thus the

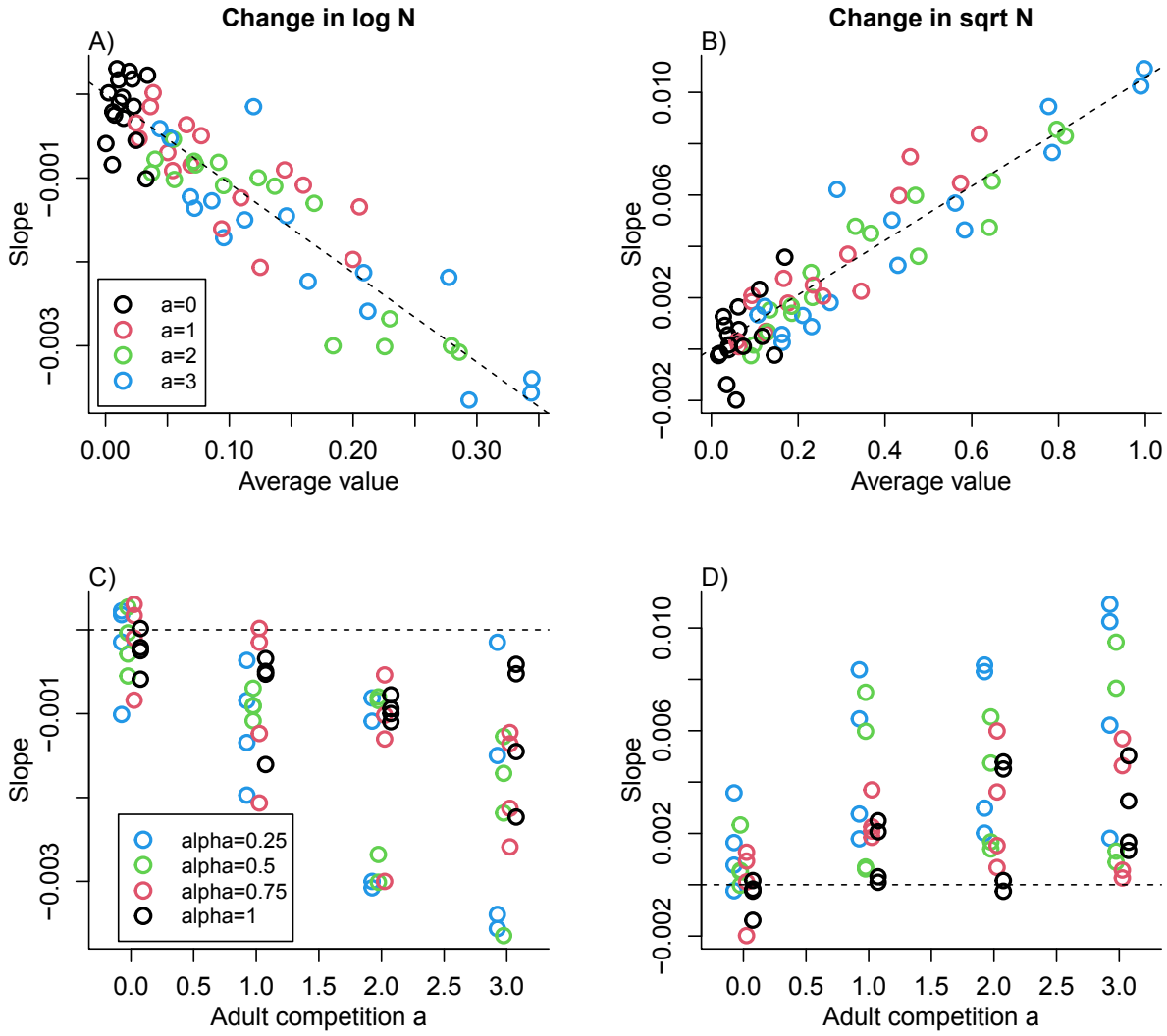

Figure S3: Summary of simulation results, as described in Fig. S2 and the text, across a range of parameter combinations: $a \in \{0,1,2,3\}$, $\alpha \in \{0.25,0.5,0.75,1\}$, $\delta \in \{0.1,0.4\}$ and other parameters as in Fig. S2. Panels A) and B) show the slope of the regression lines (as in Fig. S2 C, D) for one-step-ahead change as a function of initial population, as a function of the average one-step-ahead change, for the change in $\log N$ and $\sqrt{N}$ respectively. Dashed lines are fitted linear regressions with intercept fixed at zero. Panels C) and D) show the same slopes as a function of adult competition strength a. Figure produced by scripts `CompareClusterMetrics-loops.R` and `SlopesPlot.R` using R version 4.1.1.

largest slopes occur when intraspecific adult competition is strong (which affects the resident more than the invader) and larvae disperse widely ($\alpha = 0.25$ or 0.5). Because the dispersal kernel has a finite range cutoff, increase with N of the change in $\sqrt{N}$ cannot be an accelerating traveling wave resulting from a fat-tailed dispersal kernel. The decrease with N of the change in $\log N$ can be interpreted as approximately

exponential growth, decelerating as population density increases, so the limiting value as $N \to 0$ would be a close analog to the usual invasion growth rate for models with continuous population density.

However, we have chosen to use the average one-step increase in log$N$ for initial N in [10, 40] as our measure of the invader's initial rate of increase. The slopes are small enough that average and intercept should be similar, and the intercept of the fitted linear regression may not be representative in cases where the slope is mainly the result of density dependent effects at the upper end of N values. And as we wrote in the main text, our focus here is *how* to partition any growth rate measure for any discrete, spatial model, not on *what* to partition for any particular model.

Several studies of invader spread in discrete spatial models have observed the phenomenon of *nucleation*, meaning that small initial clusters tend to shrink, while only larger ones have the potential to grow, depending on parameter values (Allstadt et al., 2007; Gandhi et al., 1999; Korniss and Caraco, 2005; O'Malley et al., 2006). When nucleation is present, successful invasion depends on repeated introductions, until demographic stochasticity allows a cluster of invaders to reach the critical size at which expected cluster growth rate becomes positive. Nucleation would again invalidate $\mathbb{E}[r]$ as a metric of invasion success.

But we have not seen any signs of nucleation in our model, at any values of the parameters, even though it was observed by Usinowicz (2015) in a lattice lottery model nearly identical to ours. We cannot say for sure what accounts for this difference, but we suspect that it is because our model allows an invader to colonize beyond its nearest neighbor sites. Except for Usinowicz (2015), the ecological models where nucleation has been observed limit invader spread to nearest neighbor sites. Usinowicz (2015) derived a nucleation approximation for non-nearest-neighbor dispersal, but did not report any simulations with non-nearest-neighbor dispersal verifying that small clusters still tended to shrink or to grow less quickly than larger clusters.

Section S3 Sampling small invader clusters with the Fleming-Viot algorithm

The Fleming-Viot algorithm is a general method to generate samples from the *quasi-stationary distribution* of a Markov chain whose ultimate fate is to eventually enter and thereafter remain in some set of absorbing states (e.g. Asselah et al., 2011; Groisman and Jonckheere, 2013). For our model,

the absorbing states are extinction of one or the other species. The quasi-stationary distribution is the distribution of model states at large times T conditional on neither species being extinct.

The general Fleming-Viot algorithm is very simple. $N \gg 1$ independent simulations of the model are conducted in parallel up to time $T \gg 1$. If a simulation enters an absorbing state at time $t \leq T$, that move is canceled and instead that simulation's state at time t is drawn at random from the states of all simulations that are in a non-absorbing state at time t. As $T,N \to \infty$, the N simulation states at time T converge to a sample from the quasi-stationary distribution.

Fleming-Viot again encounters the problem that states where a successfully coexisting species is very rare will be very infrequent in the quasi-stationary distribution, resulting in impossibly long computing times to get the samples that we need. We therefore applied Fleming-Viot with extinction defined to occur whenever the invader abundance was far from the target range $[G_{min},G_{max}]$ within which $\mathbb{E}[r]$ is approximately constant — we call this a "quasi-extinction". So long as the quasi-extinction thresholds are far enough away from the target range of invader population sizes, the thresholds should have little effect on the quasi-stationary distribution within the target range.

Figure S4 compares four measures characterizing small invader clusters generated by the repeated invasions method described in the main text, versus the Fleming-Viot method described above, across a range of parameter values. There are no systematic differences in the one-step-ahead population growth rate, which is the key quantity for our analyses of coexistence. For the two measures of cluster structure, there may be some small systematic differences, which is not entirely surprising. In the repeated invasions method, model trajectories always enter the target range (between 10 and 40 invaders) from below. In Fleming-Viot, model trajectories rarely enter from below because the quasi-stationary distribution is concentrated near the upper quasi-extinction threshold; most enter from above, a few start within the target range. Thus, there will be more Fleming-Viot samples near the top of the target range. The small differences between Fleming-Viot and repeated invasion samples is in line with Fig. S3 showing that the mean one-step-ahead change in log invader population (i.e., $\mathbb{E}[r]$) is nearly constant as a function of cluster size within the target range.

Thus, two very different approximate but feasible ways of generating random samples of small invader clusters give nearly identical results. On that basis, we consider that it is reasonable to use either one of them.

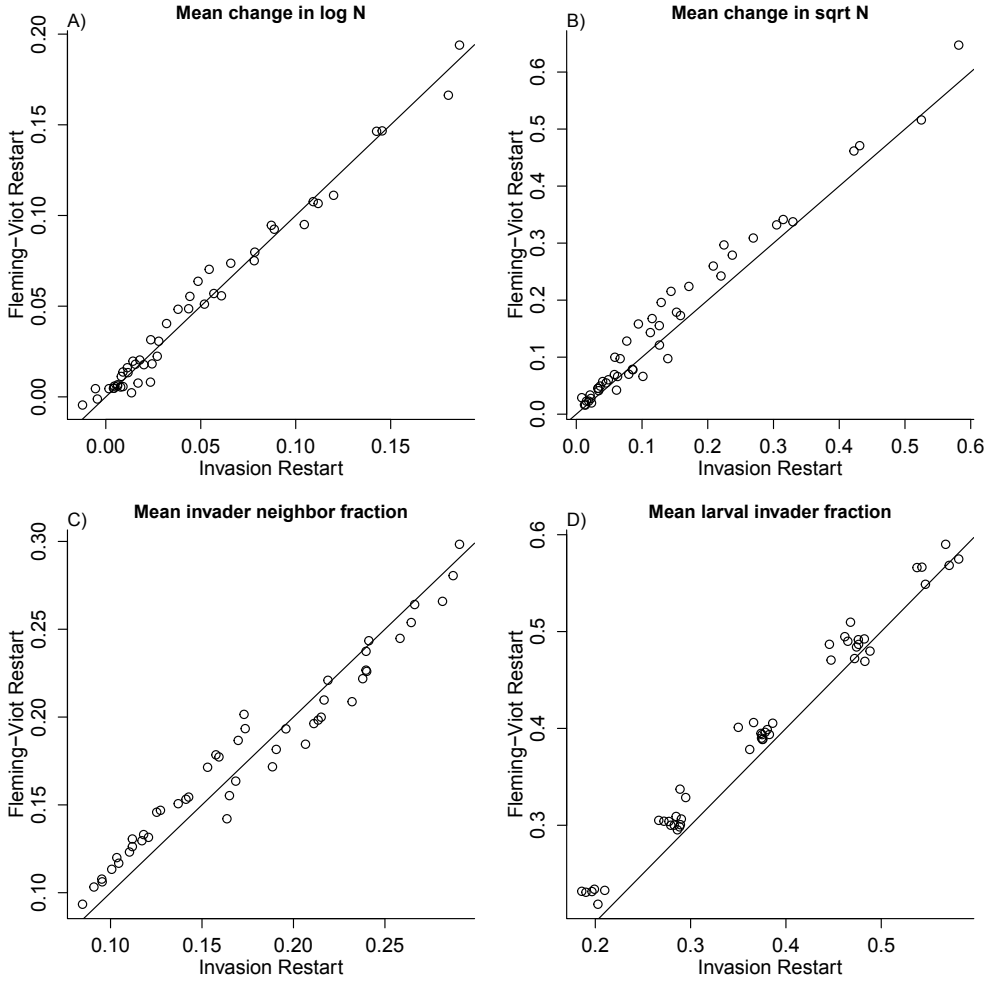

Figure S4: Comparisons between small invader clusters generated by the repeated invasions method described in the main text, with clusters generated by the Fleming-Viot simulations described in this section for all combinations of $a = 0$ or 1; α =0.5, 0.5, 0.75, or 1 for both species ; $\delta = 0.1$,0.2,4 for both species, and Moore or Moore3 adult competition neighborhoods. Demographic parameters for all simulations, were $\mathbb{E}[\log\beta]$ =0.5, 0.4 respectively for resident and invader species, with variances 0.6^2 and correlation -0.75 between $\beta_1(t)$ and $\beta_2(t)$. The panels show comparisons of A) mean one-step-ahead change in log invader total population, B) mean one-step-ahead change in square root of invader total population, C) mean fraction of invaders in an invader individual's competition neighborhood, and D) mean larval invader fraction as defined in the main text. The Fleming-Viot quasi-extinction thresholds were at total invader populations of $N = 1$ and $N = 80$, and the cluster samples were limited to total invader populations between $N = 10$ and $N = 40$. Simulations were done on a 50×50 lattice, and each plotted value is based 100 one-step-ahead simulations for each of 50 randomly generated invader clusters in the target range. Figure generated by scripts `CompareClusterSampling.R`, `ClusterSamplingComparisonPlot` and scripts that those source, using R version 4.0.2.

Section S4 Further partitioning of the contributions of variation in competition

The $\overline{C}$ counterfactual (23) washes out all information about how spatial structure affects the distribution of C values. To preserve some of that information, we can consider an intermediate counterfactual where each "real" C_q value is replaced by its average for the particular invader-resident configuration — this retains variation in average C between different configurations, but removes variance within each configuration.

The calculations are as follows. For each species, compute

$$\widehat{C}_q^{(k)}(T) = \frac{1}{VR}\sum_{v=1}^{V}\sum_{r=1}^{R} C_q^{(r|v,k)}(T). \qquad \text{(Eq. S6)}$$

Then for each (r,v,k), compute the pseudo-one-step-ahead population change as

$$N_q^{(r|v,k)}(T+1) = \left(\bar{S}_q^{(k)}(T+1) + N_q^{(k)}(T)\frac{E_q^{(r|v,k)}(T)}{\widehat{C}_q^{(k)}(T)}\right)\eta_q^{(r|v,k)}(T). \qquad \text{(Eq. S7)}$$

and compute the resulting population change measure $\chi_q^{(r|v,k)}(E,\widehat{C},\eta)$. The average of these RVK values gives the counterfactual population change measure $\overline{\chi}_q(E,\widehat{C},\eta)$.

The ε^C and resulting Δ^C term are then sub-partitioned into two pieces:

$$\varepsilon_q^C = \left[\overline{\chi}_q(\overline{E},C,\eta) - \overline{\chi}_q(\overline{E},\widehat{C},\eta)\right] + \left[\overline{\chi}_q(\overline{E},\widehat{C},\eta) - \overline{\chi}_q(\overline{E},\overline{C},\eta)\right] = \varepsilon_q^{C_w} + \varepsilon_q C_b \qquad \text{(Eq. S8)}$$

where the w and b subscripts refer to variance in C within and between invader-resident partitions.

Section S5 Detailed methods for partition based on life history differences

As in the partition based on fluctuation-dependent mechanisms, K lattice states at time T with small invader clusters (indexed by k) are generated by simulating the full model (including all life history differences), and stored — this much is identical. But then, because site vacancies depend on mortality rates that differ across different scenarios, vacancy configurations are generated anew for each counterfactual. In each

scenario, for each lattice state k, V vacancy configurations are generated using the scenario's δ values, and R one-step-ahead simulations of population change are simulated using the scenario's β values to generate population change measures $\overline{\chi}_q$, $q=1,2$. For example, $\overline{\chi}_q(\delta,\beta,\alpha)$ results from vacancies and one-step-ahead replicates where species differ in all three traits, while $\overline{\chi}_q(\overline{\delta},\overline{\beta},\overline{\alpha})$ results from vacancies and one-step-ahead replicates where species are identical in all three traits. Because demographic stochasticity is not included as a factor in the decomposition, any combination of R and V can be used such that RV is large enough to estimate average growth rates; we used $V \gg 1$ and $R=1$ as before.

The partitioning of each species' population growth rates is then

$$\begin{aligned}
\bar{\varepsilon}_q^0 &= \overline{\chi}_q(\overline{\delta},\overline{\beta},\overline{\alpha}) \\
\bar{\varepsilon}_q^\delta &= \overline{\chi}_q(\delta,\overline{\beta},\overline{\alpha}) - \bar{\varepsilon}_q^0 \text{ and analogously for } \bar{\varepsilon}_q^\beta, \bar{\varepsilon}_q^\alpha. \\
\bar{\varepsilon}_q^{\delta,\beta} &= \overline{\chi}_q(\delta,\beta,\overline{\alpha}) - (\bar{\varepsilon}_q^0 + \bar{\varepsilon}_q^\delta + \bar{\varepsilon}_q^\beta) \text{ and analogously for other pairs} \\
\bar{\varepsilon}_q^{\delta,\beta,\alpha} &= \overline{\chi}_q(\delta,\beta,\alpha) - (\bar{\varepsilon}_q^0 + \bar{\varepsilon}_q^\delta + \bar{\varepsilon}_q^\beta + \bar{\varepsilon}_q^\alpha + \bar{\varepsilon}_q^{\delta,\beta} + \bar{\varepsilon}_q^{\delta,\alpha} + \bar{\varepsilon}_q^{\beta,\alpha})
\end{aligned} \qquad \text{(Eq. S9)}$$

Like the T-partitions in Ellner et al. (2019), the counterfactuals in (Eq. S9) vary the traits, but not the biotic environment in which they operate. In this case, the biotic environment is the lattice state with small invader clusters at time T. Thus, these partitions only consider the *direct* effect of the traits on population growth, not their *indirect* effects mediated by how species' traits affect the biotic environment.

We attempted to include both direct and indirect effects by generating new lattice states at time T for each scenario's δ, β, and α values. This failed spectacularly because coexistence depends on the balance of δ and β: setting one of these to the average value breaks the tradeoff and causes one species or the other to rapidly exclude the other. Thus, there is no such thing as a "typical small invader cluster" when traits have been altered.

Section S6 Supplementary figures

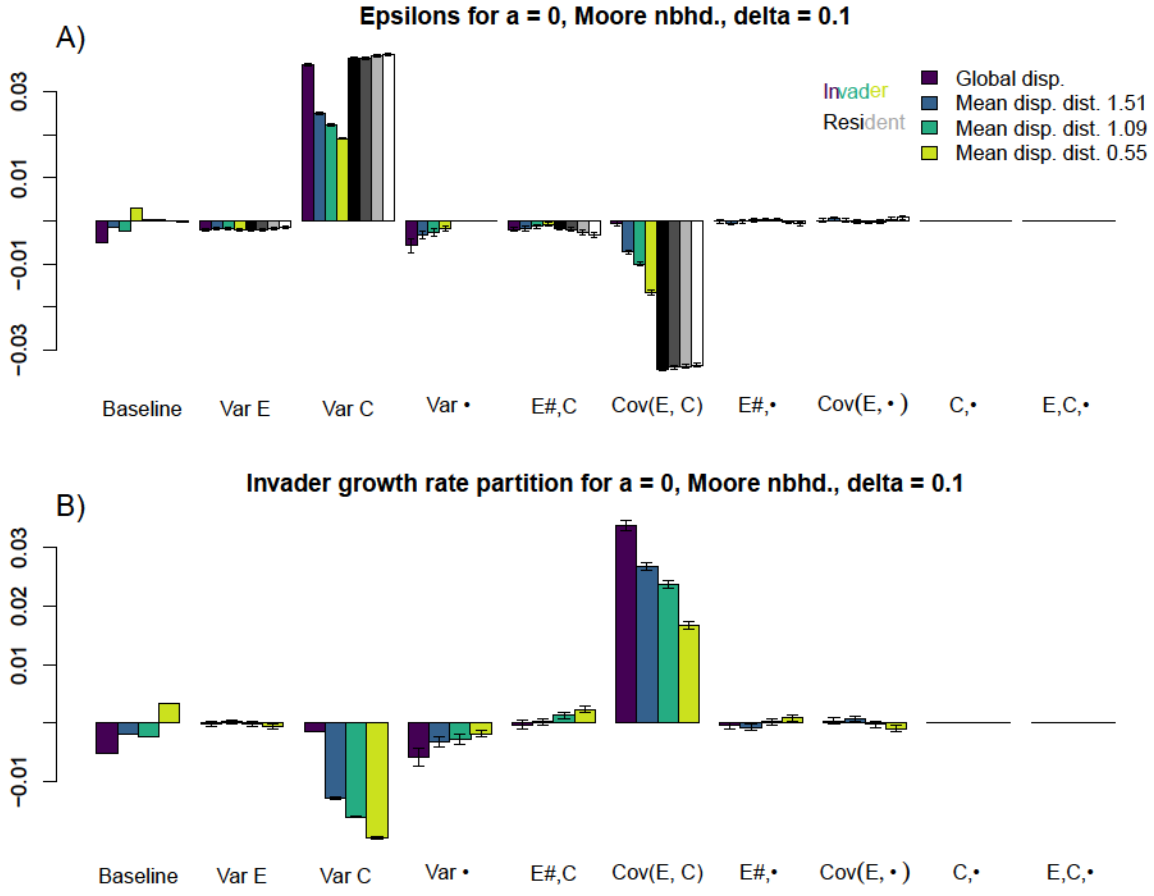

Figure S5: Barplot of partitionings for the two-species lattice lottery model with Moore competition neighborhood and death rate $\delta = 0.1$. A) $\bar{\varepsilon}$ partitioning for invader and resident. B) Δ partitioning, i.e. partition of invader growth rate into coexistence mechanisms. Lighter colors represent shorter-range dispersal, which produces more invader clustering. The mean dispersal distances for non-global dispersal correspond to α values 0.25, 0.5 and 1 in the dispersal matrix, eqn. (10). At $\alpha = 0.25$, dispersal distance $d = 4$ (the maximum possible with non-global dispersal) is $e^{-1} \approx 37\%$ as likely as distance $d = 0$. Other parameter values: $M = 50, T = 500, K = 50, R = 20, V = 50, N_{min} = 1, N_{max} = 120, G_{min} = 10, G_{max} = 40, \mu_1 = .5, \mu_2 = 0.45, \sigma_1 = \sigma_2 = 0.6, \rho = -0.75$. Figure generated by `plotDeltasVsAlpha2.R` using simulation results generated by script `latticePartitionLoops.R` and scripts that it sources using R version 4.1.1.